Nanoscale Advances

Accepted Manuscript

This article can be cited before page numbers have been issued, to do this please use: T. Goel, S. Sewariya, M. Tiwari, R. Chandra and S. Singh, *Nanoscale Adv.*, 2026, DOI: 10.1039/D6NA00034G.

ROYAL SOCIETY OF CHEMISTRY

rsc.li/nanoscale-advances

View Article Online
DOI: 10.1039/D6NA00034G

ZnO@PDA@Ag Nanocomposite-Mediated Delivery of 9-Bromonoscapine, an Anticancer Agent, for Enhanced Lung Cancer Therapy

Tanya Goel[a, c], Shubham Sewariya[b,c], Manisha Tiwari[a*], Ramesh Chandra[a,b,c*], Snigdha Singh[b,c*]

[a] *Dr. B. R. Ambedkar Center for Biomedical Research (ACBR), University of Delhi, Delhi-110007, India*
[b] *Institute of Nano Medical Sciences (INMS), University of Delhi, Delhi-110007, India*
[c] *Drug Discovery and Development Laboratory, Department of Chemistry, University of Delhi, Delhi-110007, India*

*****Corresponding author

Dr. Snigdha Singh, *M. Tech*, *Ph.D.*

Drug Discovery and Development Laboratory,
Department of Chemistry, University of Delhi, Delhi-110007
Email: ssingh3@chemistry.du.ac.in

Institute of Nano Medical Sciences (INMS),
University of Delhi, Delhi-110007, India
Email: deputydirector@inms.du.ac.in

Prof. Ramesh Chandra, *FAMS, FRSC (London)*

Institute of Nano Medical Sciences (INMS),
University of Delhi, Delhi-110007, India
Email: director@inms.du.ac.in

Drug Discovery and Development Laboratory,
Department of Chemistry, University of Delhi, Delhi-110007
Email: rchandra@chemistry.du.ac.in

Dr. B. R. Ambedkar Center for Biomedical Research (ACBR),
University of Delhi, Delhi-110007, India
Email: acbrdu@hotmail.com

Prof. Manisha Tiwari, *Ph.D.*

Dr. B. R. Ambedkar Center for Biomedical Research (ACBR),
University of Delhi, Delhi-110007, India
Email: mtiwari07@gmail.com

View Article Online
DOI: 10.1039/D6NA00034G

Abstract

Lung cancer continues to be a global threat to mankind responsible for gigantic mortalities across international boundaries, underscoring the pressing need for improved therapeutic alternatives. Recently, multifunctional nanocomposites have developed as promising platforms for anticancer therapy, offering targeted drug delivery and better intrinsic therapeutic properties owing to enhanced solubility, stability, and targeted release of hydrophobic drugs. In the present work, a biocompatible Silver-modified PDA-coated zinc oxide nanocomposite was synthesized and loaded with the hydrophobic anticancer '9-bromonoscapine' drug (9-Br-Nos) to develop 'ZnO@PDA@Ag@9-Br-Nos' nanocomposite for lung cancer treatment. The characterization of the nanocomposites was done using techniques namely DLS, TEM, Zeta Potential, FESEM-EDX, TGA, PXRD, FT-IR, which confirmed the nanocomposite's size, charge, stability, and functional integrity. Moreover, drug loading and release were quantified via high-performance liquid chromatography (HPLC), demonstrating an efficient 69.4% drug loading and sustained release of 9-Br-Nos drug at physiological pH 7.4 and enhanced release at acidic pH 5.5. The *in vitro* cytotoxicity studies revealed that ZnO@PDA@Ag@9-Br-Nos exhibited an IC_{50} of 33.51±4.54 µg/mL against H1299 lung cancer cells, while cytotoxicity tests on HEK-293 normal cells and hemocompatibility assay on human erythrocytes confirmed its biocompatibility and non-toxicity to healthy cells. These findings collectively demonstrate that ZnO@PDA@Ag@9-Br-Nos is an effective nanocarrier for hydrophobic drug delivery and shows improved therapeutic promise in the treatment of lung cancer.

Keywords: 9-Bromonoscapine, Lung cancer, Biocompatible, Zinc-Oxide nanoparticles, drug delivery

Abbreviations:

9-Br-Nos: 9-Bromonoscapine
Ag: Silver
MTT: 3-(4,5-dimethylthiazol-2-yl)-2,5-diphenyltetrazolium bromide
NSCLC: Human Non-small cell lung cancer
PDA: Polydopamine
ZnO: Zinc Oxide

View Article Online
DOI: 10.1039/D6NA00034G

$AgNO_3$: Silver Nitrate

1. Introduction

Lung cancer is among the deadliest cancers around the globe, posing a significant challenge to public health. As per the recent 2025 report by the American Cancer Society, United States, there will be approximately 2,26,650 new lung and bronchus cancer cases and around 1,24,730 deaths from this disease.[1] Globally, according to GLOBOCAN 2022, lung cancer accounted for nearly 2.48 million new cases and 1.82 million deaths, being the primary cause of cancer-related mortality for both men and women.[2] The global burden of lung cancer is expected to increase further in 2025, with an estimated 2.55 to 2.65 million new cases and roughly 1.9 million fatalities.[3,4] Lung cancer patients continue to have a minimal survival rate despite improvements in traditional chemotherapy and radiation therapy because of delayed diagnosis, multidrug resistance, and systemic toxicity.[5,6] Therefore, it is imperative to investigate new therapeutic approaches that might enhance medication effectiveness, reduce side effects, and deliver drugs precisely to the tumor sites.[7,8,9,10,11]

Nanocomposites composed of nanoscale materials can be used to develop advanced drug delivery systems.[12,13,14] They are reported to interact more effectively with the biological membranes and precisely transport drugs to targeted tumor cells, paving the way for more personalized and targeted therapies.[15,16,17] Among the diverse nanomaterials explored for biomedical applications, ZnO nanoparticles have sparked widespread interest because of their distinctive physicochemical characteristics, including high surface area, excellent biocompatibility, biodegradability, and inherent anticancer & antimicrobial activities, and are further endorsed by the U.S. FDA based on safety standards.[18,19] ZnO nanoparticles demonstrate selective toxicity towards cancer cells, making them promising candidates for combination therapies[20,21] but their application in pharmaceutics is often challenged by issues such as poor dispersion, instability in physiological environments, and rapid breakdown.[22,23] Surface functionalization of nanoparticles with various molecules such as polymers, antibodies, or drugs, also minimizes toxicity, increases dispersion, and enables controlled release of therapeutic agents, making ZnO nanoparticles more effective for applications like cancer therapy.[24,25]

View Article Online
DOI: 10.1039/D6NA00034G

In a recent study, A. Das and colleagues (2025) created a new ZnO nanocomposite that was functionalized with doxorubicin (DOX) and encapsulated in a polymethyl methacrylate (PMMA) biopolymer. The resulting DOX-ZnO-PMMA nanocomposite demonstrated improved efficacy and selectivity against 'MCF-7' breast cancer cells while reducing negative effects on healthy tissues.[26] Similarly, to enhance gemcitabine drug delivery, periodic mesoporous organosilica/zinc oxide (PMO/ZnO) nanocomposites were synthesised using rice bran extract. This system showed enhanced anticancer effects, indicating its potential as an effective targeted chemotherapy platform for cancer treatment.[27] Cisplatin (Cp) and gemcitabine (Gem) co-loaded ZnO NPs were further developed by Hu *et al.* (2020) to target non-small cell lung cancer (NSCLC) cells. These nanocomposites decreased systemic toxicity and increased drug stability, demonstrating their promise as a synergistic chemotherapy for lung cancer treatment.[28] Kazemi *et al.* (2025) synthesized metal-organic frameworks (MOFs) nanocarriers 'Zn-MOF-74' and 'RA-MOF-74' (acetate derived) at ambient temperature with increased porosity. RA-MOF-74 showed superior performance with high 5-fluorouracil (5-FU) loading, and pH-responsive release. Biocompatible ALG and PDA coatings further stabilized the nanocarrier for potential cancer therapy applications.[29] In another study, the same group developed PDA-coated Zn-MOF-74 nanocarriers with ~96% drug-loading efficiency, improved stability, and faster doxorubicin (DOX) release under acidic conditions, resulting in 85.73% inhibition of MDA-MB-231 breast cancer cells.[30]

The naturally occurring phthalide isoquinoline alkaloid, 'Noscapine' ($C_{22}H_{23}NO_7$), obtained from poppy extract is commonly used as a cough suppressant and has recently gained considerable interest as an anticancer agent against lung[31], breast[32], leukemia[33], glioma[34] and ovarian cancer[35] due to its multifaceted mechanisms of action.[35] Noscapine acts on tubulin, the building block of microtubules that are vital for proper cell division. Unlike conventional drugs that completely destabilize or rigidly stabilize microtubules, noscapine takes a gentler approach by fine-tuning their 'dynamic instability'. It slows down the normal building and breaking of microtubules inside cells, this controlled disruption interferes with normal mitotic progression, causing cells to stall at the G2/M checkpoint, limiting their ability to divide and migrate.[36,37] Studies have reported that it also reduces the levels of hypoxia-inducible factor-1 (HIF-1) and vascular endothelial growth factor (VEGF), which

View Article Online
DOI: 10.1039/D6NA00034G

are key regulators of angiogenesis. By doing so, it acts as an antiangiogenic agent, disrupting the formation of blood vessels that tumors require for grow and metastatis.[38] At the molecular level, noscapine through multiple signaling routes activates a series of caspase enzymes (caspase-2, -3, -6, -8, and -9), which execute the cell death program, while also promoting chromatin condensation and DNA fragmentation (classic hallmarks of apoptosis) that drives cancer cells toward apoptosis, or programmed cell death. In addition, it triggers the pro-apoptotic JNK pathway while suppressing ERK signaling, shifting the balance in favor of cancer cell death.[35]

Previous studies revealed that 9-Br-Nos, a halogenated derivative of noscapine, exhibits markedly greater anticancer potency than its parent compound 'noscapine'.[39,40] It effectively inhibits microtubule dynamics, cell proliferation, migration and angiogenesis at lower concentrations, and its enhanced efficacy combined with minimal toxicity highlights its promise as a superior candidate for cancer therapy.[41] Noscapine exhibited moderate anticancer effects, with IC_{50} values of 36.16 ± 3.76 μM and 42.7 ± 4.3 μM against MDA-MB-231 and MDA-MB-468 breast cancer cells.[32] Its cytotoxicity is also time-dependent, with values of 73 μM,[42] (128.82 ± 2.87) μM at 48 h and (95.81 ± 11.46) μM at 72 h against A549 lung cancer cells.[43] In comparison, noscapine derivatives such as Cl-noscapine (11.87 μM), Br-noscapine (6.9 μM), and folate-noscapine (6.79 μM) demonstrated markedly higher potency. These derivatives not only suppress proliferation more effectively but also inhibit angiogenesis, cord formation, and cell migration/invasion, underscoring their superior therapeutic promise.[40] Both noscapine and its derivative 9-Br-Nos exhibit promising anticancer activities but are constrained by specific limitations. Noscapine suffers from relatively low potency, poor water solubility, and a short biological half-life, necessitating higher or more frequent dosing.[35] 9-Br-Nos, despite showing improved potency, still faces hurdles such as limited solubility, stability concerns, rapid metabolism, non-specific distribution and insufficient clinical data on long-term safety or resistance mechanisms.[44]

Bhoi *et al.* (2025) prepared a methyl-*β*-cyclodextrin inclusion complex of 9-bromo-noscapine to improve its aqueous solubility and therapeutic performance. The optimized formulation produced stronger growth inhibition in MDA-MB-231 and MCF-7 cells, with IC_{50} values of 12.87 μg/mL and 13.07 μg/mL, respectively.[45] In another study, Jyoti *et al.*

View Article Online
DOI: 10.1039/D6NA00034G

(2015) developed inhalable 9-bromo-noscapine nanostructured lipid particles for targeted pulmonary delivery. The formulation demonstrated enhanced cellular uptake, apoptosis induction, and superior anticancer activity against A549 when compared with the free drug.[39] While 9-Br-Nos represents a significant advancement over noscapine, both compounds require optimized drug delivery strategies to overcome pharmacokinetic and formulation challenges before reaching full clinical potential.[7]

To address these limitations, this study aims to utilize water dispersible ZnO@PDA@Ag nanocomposites as a multifunctional platform for 9-Br-Nos drug delivery to achieve sustained and targeted drug release, thereby enhancing therapeutic efficacy. ZnO serves as the core material, providing a nanoscale platform with inherent anticancer potential and pH-responsive drug release tailored to the acidic tumor microenvironment.[46,47] The PDA coating forms a biocompatible interface that enhances colloidal stability and facilitates efficient drug loading *via* π–π stacking and hydrogen bonding. The incorporation of silver (Ag) on the ZnO@PDA nanocomposite contribute additional therapeutic effects and enhance cytotoxicity through synergistic interactions.[48] Furthermore, the incorporation of 9-Br-Nos, a poorly water-soluble anticancer agent, benefits from improved aqueous dispersion, sustained release within this nanocarrier system, and cytotoxicity against lung cancer cells leading to improved therapeutic performance. The synthesized ZnO@PDA@Ag@9-Br-Nos nanocomposites were characterized for their physicochemical properties and further evaluated for their anticancer efficacy against H1299 lung cancer cells, including effects on proliferation and migration. Biocompatibility was confirmed through hemolysis of RBCs and normal cell toxicity assessments on HEK-293 cells, ensuring safety for therapeutic applications. By addressing the limitations of conventional drug delivery methods and leveraging the synergistic properties of the nanocomposite components, this work highlights the potential of ZnO@PDA@Ag@9-Br-Nos nanocomposites as a reproducible, and highly effective nanoplatform for lung cancer therapy, offering prospects for future clinical translation.

2. Experimental Section

2.1. Materials and Reagents

View Article Online
DOI: 10.1039/D6NA00034G

$ZnCl_2$ (≥ 98% purity, Sigma-Aldrich); $AgNO_3$ (≥ 99.0% purity, Cas No: 7761-88-8, Sigma-Aldrich); Dopamine Hydrochloride (extrapure 98%, Cas No: 62-31-7, M.W: 189.64, SRL); S, R-Noscapine (≥ 98% purity, Cas No: 128-62-1, Sigma-Aldrich); and Thiazolyl Blue Tetrazolium Bromide dye (98% purity, Cas No: 298-93-1, Sigma) were purchased for experimental work. Phosphate-buffered saline (1x PBS, pH 7.4), Tris Buffer (pH 8.5) and '9-Br-Nos' were prepared in laboratory. Throughout, milli-Q water (>18.2 MΩ.cm) was utilized throughout all synthesis and washing steps. All additional solvents and chemicals employed in the study were analytical or HPLC grade (≥ 99.9%, Merck), depending on the experimental needs. The synthesized ZnO@PDA@Ag@9-Br-Nos nanocomposites and 9-Br-Nos were kept at 4 °C for long-term storage.

2.2. Preparation of ZnO@PDA@Ag nanocomposite

The synthesis of Silver functionalized Polydopamine-coated Zinc Oxide nanocomposite, as described in our previous work[48], involved a multi-step process and was performed following a reported method. Initially, ZnO nanoparticles were synthesized by adding 0.2 M sodium hydroxide dropwise to an aqueous solution of zinc chloride, followed by continuous stirring at 60 °C until white precipitation occurred. The precipitate was centrifuged, washed, dried and calcined at 250 °C for 3 h. The ZnO NPs (150 mg) were then coated with polydopamine (PDA) by using Tris buffer (0.01 M, pH 8.5), along with Dopamine HCl (150 mg), and stirring at 50 °C overnight. The resulting black-colored ZnO@PDA were filtered, washed, and dried. Finally, silver (Ag) doping was achieved by dispersing the ZnO@PDA NPs in milli-Q water, followed by the dropwise addition of 0.5 M silver nitrate solution and continuous stirring overnight in the dark. The successful reduction of Ag^+ to metallic Ag^0 and its anchoring onto the ZnO@PDA surface was confirmed by XPS analysis in our previous study.[48] The resulting black-colored 'ZnO@PDA@Ag' nanocomposite was collected by filtration, washed with milli-Q water and acetone, and dried in an oven at 60 °C.[48,49]

2.3. Synthesis of '9-Br-Nos' anticancer drug

As per the reported procedure, Noscapine (1.0 eq.) was dissolved in minimal amount of HBr and subsequently, a solution of Br_2/H_2O (0.2 mL/10 mL) was added to the reaction mixture dropwise using additional funnel at 0-5 ℃. After complete addition of the Br_2/H_2O solution, the reaction mixture was made to stir at RT overnight for 12 h. The reaction progress was

View Article Online
DOI: 10.1039/D6NA00034G

monitored by TLC and upon completion of the reaction, the organic layer was extracted by adding chloroform 2-3 times (brine work-up). The filtrate was dried over anhydrous Na_2SO_4 and evaporated using a rotatory evaporator to give the crude product. Finally, the crude was purified by column chromatography on alumina in 5-10% EtOAc: Hexane to give the desired 9-Br-Nos as yellowish brown crystalline solid in 97% yield. The complete structural and purity confirmation characterization of 9-Br-Nos are included in Supplementary Information (Figure S1-S3).

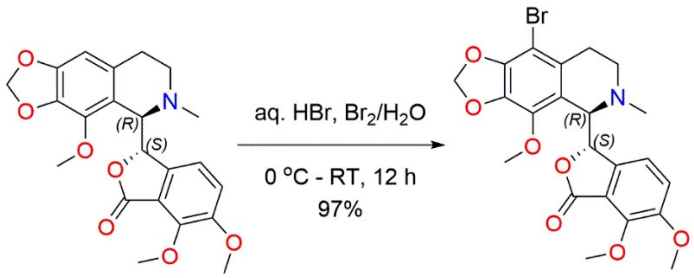

Scheme 1. Synthesis of 9-Br-Nos

2.4. Synthesis of 9-Br-Nos drug loaded ZnO@PDA@Ag nanocarriers

ZnO@PDA@Ag nanocomposites (50 mg) were vigorously stirred for 30 min in 10 mL milli-Q water, followed by dropwise addition of 9-Br-Nos solution (50 mg in 2 mL DMSO). The suspension was stirred overnight at RT in dark. The nanocomposites were centrifuged and separated at 8000 rpm for 10 min. The product was washed with milli-Q water and acetone to remove the excess extract components. Finally, ZnO@PDA@Ag@9-Br-Nos nanocomposites were obtained after overnight drying at 50 ^oC and were stored at 4 ^oC.

3. Characterization of synthesized ZnO@PDA@Ag@9-Br-Nos nanocomposite

3.1. Powder X-Ray diffraction pattern (PXRD)

The crystalline nature of the nanocomposite was confirmed using a Rigaku Ultima IV X-ray diffractometer. The instrument employed Ni-filtered Cu Kα radiation, operating at a voltage of 40 kV and current of 40 mA. Data were collected by scanning at a rate of 1°/min over a diffraction angle (2θ) range of 10° to 50°. The crystal lattice structures of the ZnO@PDA@Ag and ZnO@PDA@Ag@9-Br-Nos nanocomposites were successfully characterized through this analysis.

3.2. Fourier-Transform Infrared (FT-IR) Spectroscopy

View Article Online
DOI: 10.1039/D6NA00034G

About ~2-3 mg of powdered samples of ZnO@PDA@Ag and ZnO@PDA@Ag@9-Br-Nos nanocomposites were analyzed using a Shimadzu II FT-IR Spectrometer. The spectra were recorded across the range of 400-4000 cm^{-1} to identify and understand the functional groups and compositional characteristics of the nanocomposites, providing insight into their chemical structure and bonding.

3.3. Dynamic Light Scattering (DLS) and Zeta Potential (ζ)

A solution of ZnO@PDA@Ag@9-Br-Nos nanocomposites in milli-Q water (1 mg/mL) was prepared. The sample was sonicated for 15-20 min to ensure proper dispersion before being transferred into a quartz cuvette for analysis. The nanocomposite size distribution and surface charge were measured using SZ-100V2 Series Nanoparticle Analyzer (HORIBA Scientific, Japan).

3.4. Electron microscopy

3.4.1. Transmission Electron Microscopy (TEM) Analysis

Transmission Electron Microscopy (TEM) was used to determine the size and morphology of synthesized ZnO@PDA@Ag@9-Br-Nos nanocomposite. For TEM sample preparation, carbon-coated copper grids (PELCO®, Ted Pella Inc., USA) were used. Nanocomposites (0.5 mg) was diluted with 70% Ethanol and sonicated for 30 min before depositing on grids. The prepared sample was dried well for analysis by High Resolution Transmission Electron Microscope. Image J software (Fiji, NIH, USA) was used to calculate the average size of nanocomposite.

3.4.2. Field Emission Scanning Electron Microscopy (FESEM), Energy Dispersive X-ray Spectroscopy (EDX) Analysis and Elemental Mapping

The surface morphology, elemental composition and mapping of ZnO@PDA@Ag@9-Br-Nos nanocomposites were examined by FESEM-EDX using a Zeiss GeminiSEM 500 thermal field emission microscope. An aq. suspension of ZnO@PDA@Ag@9-Br-Nos nanocomposites (1 mg/mL) was sonicated, drop-cast onto a glass slide, and dried for analysis.

3.5. Estimation of *in vitro* 9-Br-Nos drug loading and release efficiency using High Performance Liquid Chromatography (HPLC)

View Article Online
DOI: 10.1039/D6NA00034G

Reverse phase HPLC analysis was done to determine the drug loading content and *in vitro* release efficiency of 9-Br-Nos using a Dionex Ultimate 3000 system (Thermo Scientific, USA) having a photodiode array detector. Data acquisition and processing were carried out with Chromeleon software version 6.80 SR13 (Dionex, USA). HPLC-grade acetonitrile and water were sonicated and filtered through 0.25 µm nylon membranes prior to use. A 2 mg/mL stock solution of 9-Br-Nos was prepared, from which working standards of 100, 150, 200, 300, and 400 µg/mL were obtained to construct the calibration curve. All samples were filtered through 0.25 µm filters, and 20 µL aliquots were injected for analysis. Chromatographic separation was achieved on a Thermo Scientific™ Acclaim™ 120 C18 column (250 × 4.6 mm, 5 µm particle size) using acetonitrile: water (65:35, v/v) as the mobile phase at a flow rate of 1 mL/min. The total run time was 6 min/sample, and detection was carried out at wavelength of 272 nm. The percentage of drug loading (DL) was calculated using the following equation:

$$\%\ Drug\ Loading = \frac{Weight\ of\ 9{-}Br{-}Nos\ Drug\ in\ Nanocomposite}{Weight\ of\ ZnO@PDA@Ag@9{-}Br{-}Nos\ Nanocomposite}\ x100 \quad (1)$$

The *in vitro* '9-Br-Nos' drug release from ZnO@PDA@Ag@9-Br-Nos nanocomposite was carried in 1x PBS (pH 7.4) and was measured for 48 h. 1 mg/mL of nanocomposite with bound 9-Br-Nos drug solution was transferred in a dialysis bag (MWCO: 12 kDa, flat width 25 mm; Sigma-Aldrich, St. Louis, MO, USA). The dialysis bag was then immersed in a beaker containing a magnetic bead in 1x PBS, stirred at 600 rpm, and the temperature was maintained at 37°C ± 5 °C. After different interval of time (0, 2, 4, 6, 8, 12, 24, and 48 h), 5 mL samples were withdrawn and the same volume was replaced by fresh 1x PBS. The samples were filtered through 0.25 µm filters before analysis by HPLC to find the concentration of released 9-Br-Nos drug. The release kinetics was expressed by plotting % drug release from the nanocomposite against time.

4. Cellular Experiments

The H1299 cell line was used as an *in vitro* model for lung cancer due to its origin from human non-small cell lung carcinoma (NSCLC). It exhibits a p53-null status, which is associated with aggressive tumor behavior and reduced responsiveness to standard

View Article Online
DOI: 10.1039/D6NA00034G

treatments. These characteristics makes H1299 an appropriate and widely accepted model for assessing the effectiveness of new anticancer agents and nanocarrier-based drug delivery systems. Human embryonic kidney cells 'HEK-293' served as the non-cancerous control to assess biocompatibility of the nanocomposite. Both cell lines were obtained from the National Centre for Cell Science (NCCS), Pune, India and cultured in Dulbecco's Modified Eagle Medium (DMEM) supplemented with 10% fetal bovine serum (FBS) and 1% penicillin-streptomycin. The cells were maintained at 37 °C in a humidified atmosphere containing 5% CO_2 and sub-cultured at 70-80% confluency.

4.1. Cytotoxicity analysis by MTT Assay

The cytotoxic evaluation of ZnO@PDA@Ag@9-Br-Nos nanocomposite was performed using the H1299 lung cancer cell line and the normal HEK-293 cell line. Both the cells were grown in DMEM media and were maintained in incubator. The H1299 and HEK-293 cells were seeded to 96 well plates at a density of $8x10^3$ cells/well and $15x10^3$ cells/well respectively, and was allowed to grow for 24 h. An aqueous solution of ZnO@PDA@Ag@9-Br-Nos nanocomposites (2 mg/mL) was prepared and sonicated for 10 min. The cells were then treated with varying concentrations of this stock (2, 10, 20, 40, 60, 80 and 100 µg/mL) and incubated for 48 h to assess the cytotoxic effects. 10 mg/mL concentration of 9-Br-Nos drug in DMSO solvent was used as a positive control in the experiment. Following the completion of incubation period, 20 µL of MTT reagent (5 mg/mL stock solution) was added to each well, which was then further incubated for 3 h in a CO_2 incubator at 37 °C. After the incubation, MTT reagent was discarded and 100 µL DMSO was used to dissolve the formed formazan crystals. Spectrophotometric measurement of the color's intensity reveals a proportional relationship between it and the quantity of viable cells. The absorbance value was recorded using a BioTek 800 TS microplate reader at 570 nm and reference at 630 nm. The effect of the ZnO@PDA@Ag@9-Br-Nos nanocomposites on the H1299 and HEK-293 cell proliferation was expressed as the % Cell Viability, using the following formula:

$$\%\ Cell\ Viability\ = \frac{OD\ (570-630)treament}{OD\ (570-630)control} \times 100 \qquad (2)$$

4.2. Nanoparticle-Induced Morphology Changes in H1299 Cells

View Article Online
DOI: 10.1039/D6NA00034G

To assess the morphological changes in H1299 cells due to the drug and nanocomposite, the cells were seeded in 6-well plates at a density of 5×10^5 cells/well. Following a period of 24 h, the cells were treated with 9-Br-Nos drug and ZnO@PDA@Ag@9-Br-Nos nanocomposites with their respective IC_{50} values. A phase-contrast inverted microscope at 20× magnification was used to examine cellular morphology and assess structural alterations caused by drug and nanocomposites treatments after 48 h.

4.3. Clonogenic Survival Assay

For Cell proliferation analysis, H1299 cells (1500 cells/well) were seeded in 6 well plates and stabilized in a CO_2 incubator. After 24 h of incubation, cells were treated with sub-IC_{50} concentrations of 0, 5, 15, 25 µg/mL of ZnO@PDA@Ag@9-Br-Nos nanocomposites. The media was changed into fresh media after 24 h of treatment, and cells were cultured for a week. The cells were washed twice with PBS for 3 min each, then fixed with methanol for 5 min at RT. After fixation, they were again washed twice with 1x PBS for 3 min and subsequently stained with 0.1% crystal violet solution for 30 min at RT. The Colonies were imaged after washing with water to remove any excess CV and colonies were counted using Image J software (Fiji, NIH, USA). Data were plotted using GraphPad Prism 8.4.2, and results were analyzed by Dunnett's multiple comparisons test. For clonogenic assay, the percentage of colony formation was calculated using the following formula:

$$\%\ Colony\ Formation = \frac{No.\ of\ colonies\ in\ treatment}{No.\ of\ colonies\ in\ control} x\ 100 \quad (3)$$

4.4. Migration Inhibition Potential Assay

A wound healing assay was employed to evaluate the migration potential of treated and untreated H1299 cells. The cells were allowed to grow in 6 well plate, with 1×10^6 cells/well in 2 mL of growth DMEM medium and incubated until ~90-95% of confluency is achieved. The cell monolayer was scratched in a single direction using a sterile 200 µL pipette tip to create a uniform wound and then the wells were washed with 1x PBS twice to remove detached cells from the plates. Cells were kept in incubator at 37 °C for 24 h with or without treatment with sub-IC_{50} concentrations of 0, 5, 15, 25 µg/mL ZnO@PDA@Ag@9-Br-Nos nanocomposites in DMEM medium. After 24 h of incubation, the wound gap was imaged using a phase-contrast inverted microscope at 20× magnification and quantitatively analyzed

View Article Online
DOI: 10.1039/D6NA00034G

with ImageJ software (Fiji, NIH, USA). For migration assay, the percentage of wound closure was calculated using the following formula:

$$\%\ Cell\ Migration = \frac{No.\ of\ migrated\ cell\ in\ treatment}{No.\ of\ migrated\ cells\ in\ control} x\ 100 \quad (4)$$

4.5. Flow Cytometry Apoptosis Analysis

To evaluate cell apoptosis, H1299 cells were collected from untreated cells, and treated with 9-Br-Nos drug (10 µg/mL) and ZnO@PDA@Ag@9-Br-Nos nanocomposite (~IC_{50} concentration). Following 48 h of treatment, H1299 cells were harvested from each well using Trypsin-EDTA and washed with 1x PBS. Flow cytometry analysis was conducted using an Annexin V-APC/7-AAD Apoptosis Detection Kit. The cells were re-suspended in 150 µL of Annexin V binding buffer containing 2.5 µL of Annexin V-APC and incubated in dark for 30 min at room temperature. Then, the cells were washed and re-suspended in 500 µL of binding buffer containing 2.5 µL of 7-AAD and incubated in darkness for 15 min. Flow cytometry analysis was perfomed using BD FACSymphony™ S6 instrument, determined the percentage of apoptotic cells. Annexin V-APC was detected in APC channel while 7-AAD was detected in PE/Cy5 channel. The results obtained were analysed using BD FACSDiva 9.5.1 software.

4.6. *In vitro* Hemocompatibility Assessment by Hemolysis Assay

The hemolytic activity of the ZnO@PDA@Ag@9-Br-Nos nanocomposite was evaluated using freshly collected human erythrocytes (RBCs). To separate RBCs, whole blood taken from a healthy volunteer was washed thrice with phosphate-buffered saline (1x PBS, pH 7.4) and centrifuged at 3500 rpm for 5 min. The RBC pellet formed was diluted with 1x PBS to obtain a 4% RBC suspension. 100 µL of different concentrations of ZnO@PDA@Ag@9-Br-Nos nanocomposite suspension (30, 150, 250, 350, 450, 550, and 650 µg/mL) were incubated with 100 µL of diluted RBC suspension at 37 °C for an hour. 1x PBS served as the negative control (0% hemolysis), while 1% Triton X-100 was used as the positive control (100% hemolysis).

Following incubation, the samples were centrifuged at 3500 rpm for 10 min, and the resulting supernatants were collected in a 96-well plate. Absorbance was recorded at 405 nm using a BioTek 800 TS microplate reader. Hemolysis (%) was determined using the formula below and plotted as a function of nanocomposite concentration (µg/mL):

View Article Online
DOI: 10.1039/D6NA00034G

$$\% \, Hemolysis = \frac{OD\ (test) - OD\ (negative)}{OD\ (positive) - OD\ (negative)} X\ 100 \qquad (5)$$

4.7. Statistical analysis

All biological experiments were done in triplicate (n = 3), and the results are provided as mean ± SD. The Graphs were plotted using GraphPad Prism 8.4.2 and the statistical analysis was carried out using one-way ANOVA followed by Dunnett's of or Tukey's multiple comparisons test to evaluate the significance between each treatment group and the control. Statistical significance was considered at $p < 0.05$. Levels of significance were reported as follows: p* < 0.05, p** < 0.01, p*** < 0.001, and p**** < 0.0001.

5. Result and Discussion

5.1. Characterization of synthesized ZnO@PDA@Ag@9-Br-Nos nanocomposite

5.1.1. Powder X-ray diffraction pattern (PXRD)

The chemical nature of the so formed nanocomposites 'ZnO@PDA@Ag' and 'ZnO@PDA@Ag@9-Br-Nos' was evaluated through Powder X-ray diffraction analysis. XRD peaks obtained at 2θ values were 31.84°(100), 34.44°(002), 36.32°(101), 46.28°(102), 56.70°(110), 62.92°(103), 67.98°(112) which correspond to ZnO peaks indicating the wurtzite hexagonal structure and the 2θ values 38.16°(111), 44.36°(200), 64.56°(220), 77.46°(311) correspond to Ag peaks.[48,50] XRD determined the crystalline nature of the synthesised nanoparticle, lattice planes (100), (002), (101), (111) indicate the presence of pure form of nanocomposite as shown in (**Figure 1**). However, upon the addition of '9-Br-Nos' drug to the ZnO@PDA@Ag nanocomposite, the peak's strength was reduced as compared to the nanoparticles itself. The decrease in XRD peak intensity resulted from drug-nanocomposite interactions that alter the crystal structure or surface chemistry.[51]

View Article Online
DOI: 10.1039/D6NA00034G

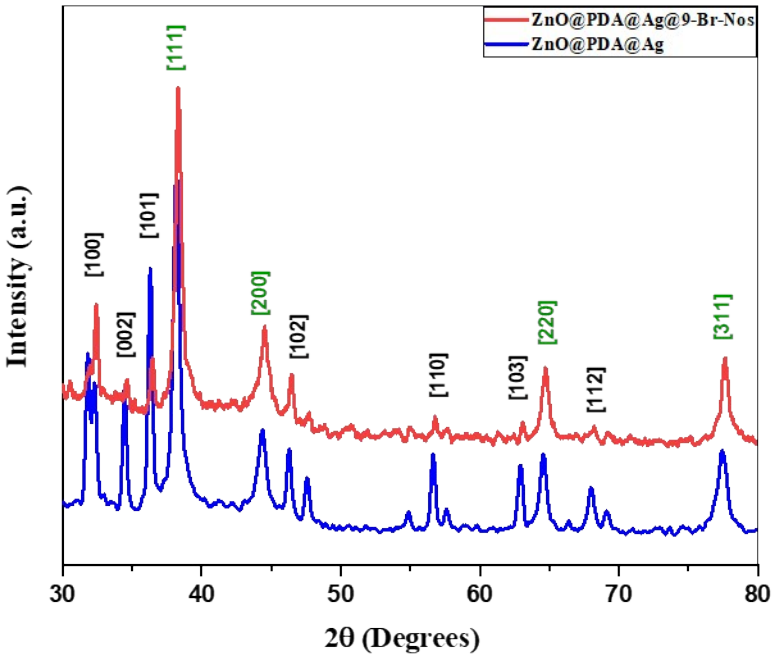

Figure 1. PXRD of ZnO@PDA@Ag and ZnO@PDA@Ag@9-Br-Nos nanocomposites

5.1.2. Fourier-Transform Infrared (FT-IR) Spectroscopy

FT-IR was used to study the successful immobilization of various functionalities at each step of nanocomposite preparation. The stretching frequency of ZnO@PDA@Ag as well as ZnO@PDA@Ag@9-Br-Nos have been recorded in the range 400-4000 cm^{-1} (**Figure 2**). The bonds that appeared at 3443 cm^{-1} correspond to stretching of the O-H group of absorbed water on the surface. The peak located at 1379 cm^{-1} was attributed to the bending vibration of C-H in the methyl group. The absorption band at 464 cm^{-1} was attributed to the stretching mode of Zn-O.[52] The broad peaks at PDA peaks located at 1284, 1490, 1579, 3452 cm^{-1} correspond to C–O, C=N or/and C=C, C=O and –OH or/and N–H vibrational modes.[53] The 9-Br-Nos drug exhibited characteristic peaks at 2922, 1747, 1440, 615 correspond to C-H stretching vibration, C=O, N-CH_3, and C-Br groups.[39]

View Article Online
DOI: 10.1039/D6NA00034G

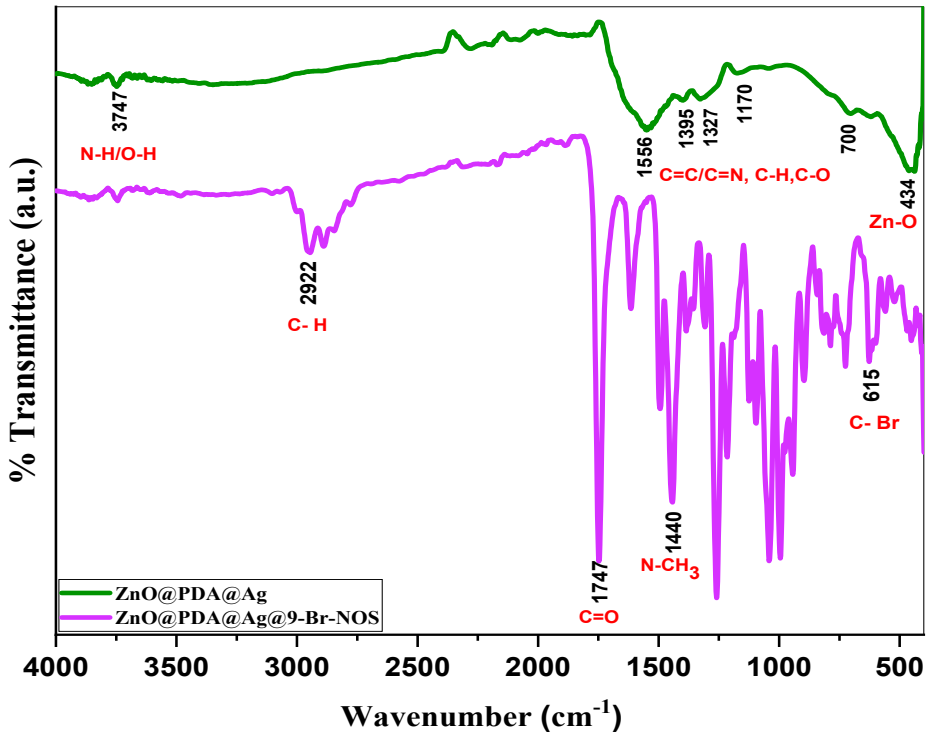

Figure 2. FT-IR Spectra of ZnO@PDA@Ag and ZnO@PDA@Ag@9-Br-Nos nanocomposites

5.1.3. Dynamic Light Scattering (DLS) and Zeta Potential (ζ)

Using DLS and zeta potential measurements, the ZnO@PDA@Ag@9-Br-Nos nanocomposite's hydrodynamic size and surface charge were assessed. The DLS results **(Figure 3a)** showed a narrow size distribution with a hydrodynamic diameter of ~80.7 nm and polydispersity index (PDI) value of 0.502, indicating a single size population with relatively moderate polydispersity and well-dispersed nanocomposites in water. The relatively small and consistent particle size suggested that the PDA coating, along with the Ag doping and 9-Br-Nos loading, did not cause significant aggregation, which is important for maintaining colloidal stability and promoting cellular uptake in biological systems.

A surface charge of -31.5 mV was found by zeta potential measurement **(Figure 3b)**, suggesting that the nanocomposite suspension was strongly electrostatically stabilized. A zeta potential magnitude above ± 30 mV is typically considered to prevent particle aggregation via electrostatic repulsion, confirming the excellent colloidal stability of the ZnO@PDA@Ag@9-Br-Nos nanocomposite. Additionally, the negative surface charge may influence interactions with cell membranes and biomolecules, which is crucial for effective drug delivery.

View Article Online
DOI: 10.1039/D6NA00034G

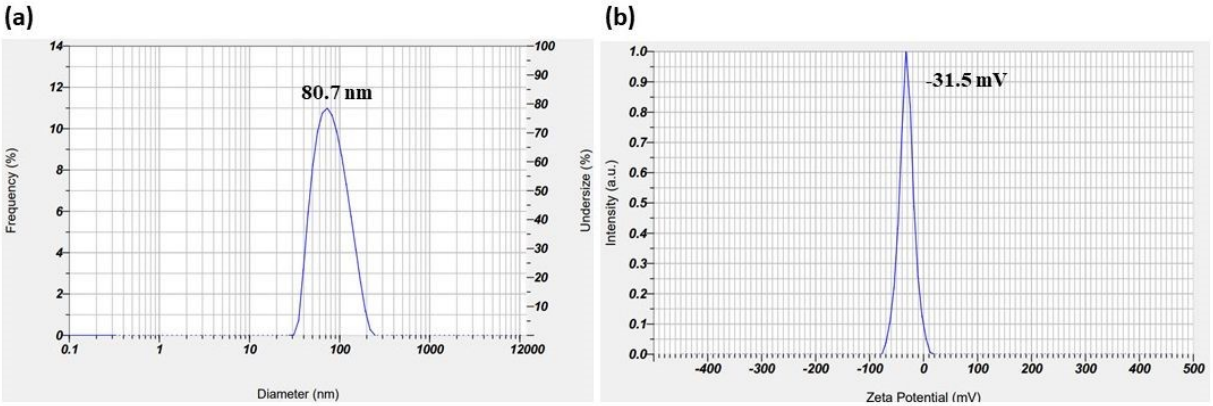

Figure 3. (a) DLS and (b) Zeta Potential of ZnO@PDA@Ag@9-Br-Nos nanocomposites

5.1.4. Electron microscopy

5.1.4.1. Transmission Electron Microscopy (TEM) Analysis

The morphology and structural features of the synthesized ZnO@PDA@Ag@9-Br-Nos nanocomposite were investigated using TEM. The low- and high-magnification TEM images as shown in **Figures 4(a, b)** displayed the nearly spherical nanocomposites with slight aggregation and a clear contrast between the darker ZnO core and lighter PDA shell, confirming a core–shell structure. **Figure 4c**, represents the SAED pattern exhibiting concentric diffraction rings indexed to wurtzite ZnO and fcc Ag, indicating a polycrystalline nature. Particle size distribution **(Figure 4d)** showed sizes between 30-80 nm with a mean diameter of 46.40 ± 1.01 nm, reflecting uniformity and controlled synthesis. The observed structural features and nanoscale dimensions are expected to support improved cellular uptake, highlighting their potential for biomedical applications.

View Article Online
DOI: 10.1039/D6NA00034G

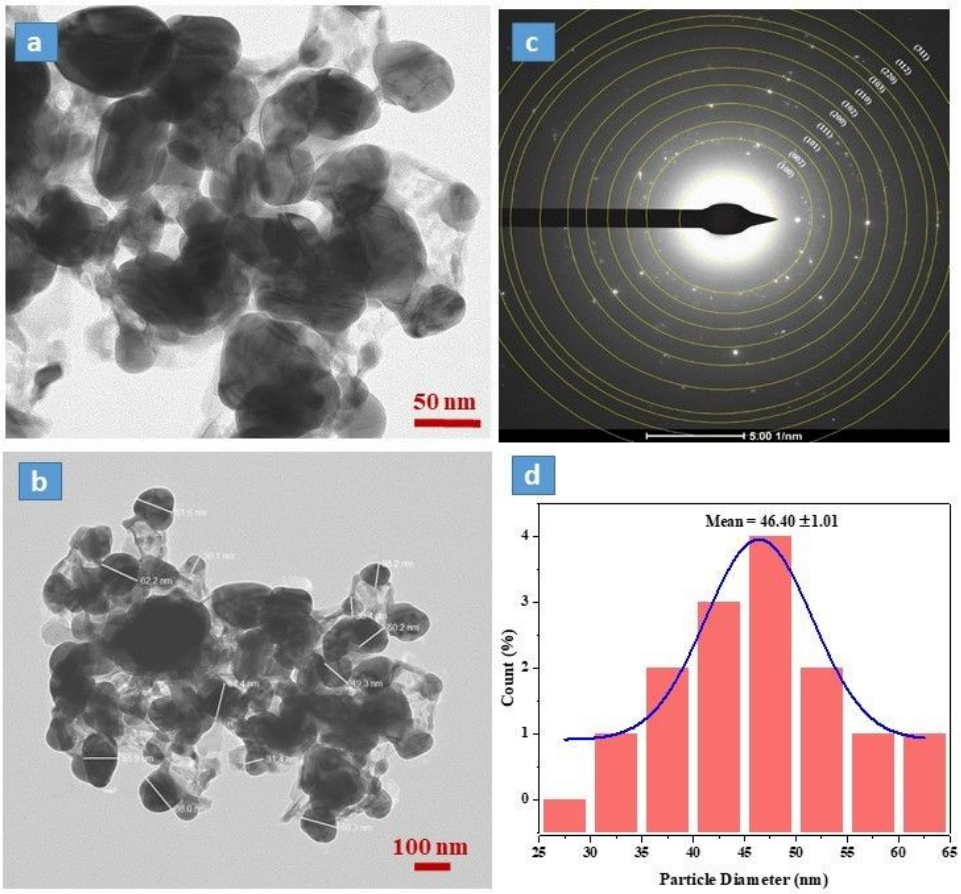

Figure 4. TEM images of ZnO@PDA@Ag@9-Br-Nos nanocomposites at (a) 50 nm and (b) 100 nm; (c) SAED pattern & (d) Histogram representing mean particle diameter

5.1.4.2. Field Emission Scanning Electron Microscopy (FESEM), Energy Dispersive X-ray Spectroscopy (EDX) Analysis and Elemental Mapping

The FESEM images of ZnO@PDA@Ag@9-Br-Nos nanocomposites as shown in **Figure 5 (a-c)** were taken at different scales 1 µm, 100 nm and 200 nm and magnification of 30 KX, 100 KX, and 75 KX respectively, suggesting that the nanocomposites have a roughly spherical shape and are present in chain like confirmation.

View Article Online
DOI: 10.1039/D6NA00034G

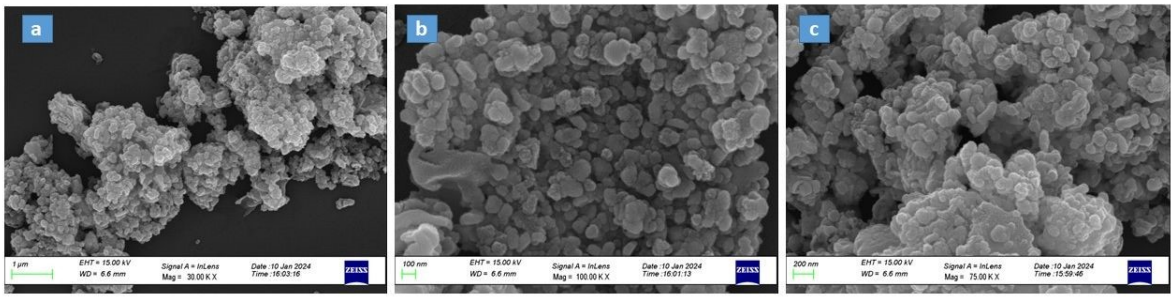

Figure 5. FESEM images of ZnO@PDA@Ag@9-Br-Nos nanocomposites at (a) 1µm, (b) 100 nm, and (c) 200 nm

The EDX analysis of ZnO@PDA@Ag@9-Br-Nos nanocomposite displayed the presence of elements like Carbon (C), Nitrogen (N), Oxygen (O), Bromine (Br), Silver (Ag) and Zinc (Zn) in 21.18 wt %, 0.21 wt %, 7.88 wt %, 5.43 wt %, 27.64 wt %, and 37.69 wt % respectively as shown in **(Figure 6)**. The presence of Bromine confirmed the successful loading of 9-Br-Nos drug on the nanocomposite. Also, the elemental mapping performed confirmed the homogenous distrubution of the constituent elements throughout the nanocomposite **(Figure 7)**.

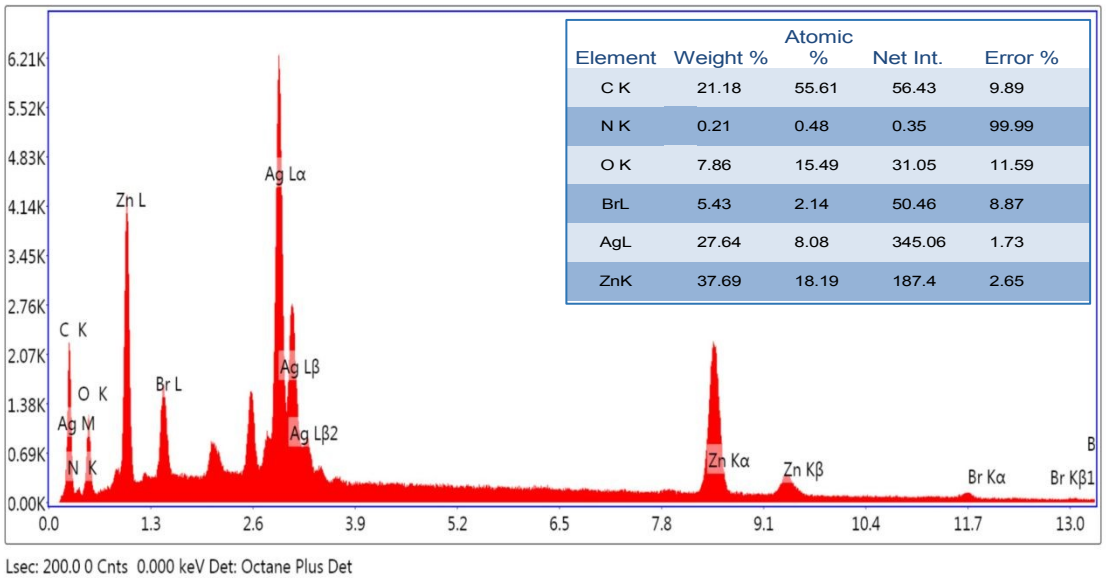

Figure 6. EDX analysis of ZnO@PDA@Ag@9-Br-Nos nanocomposite

View Article Online
DOI: 10.1039/D6NA00034G

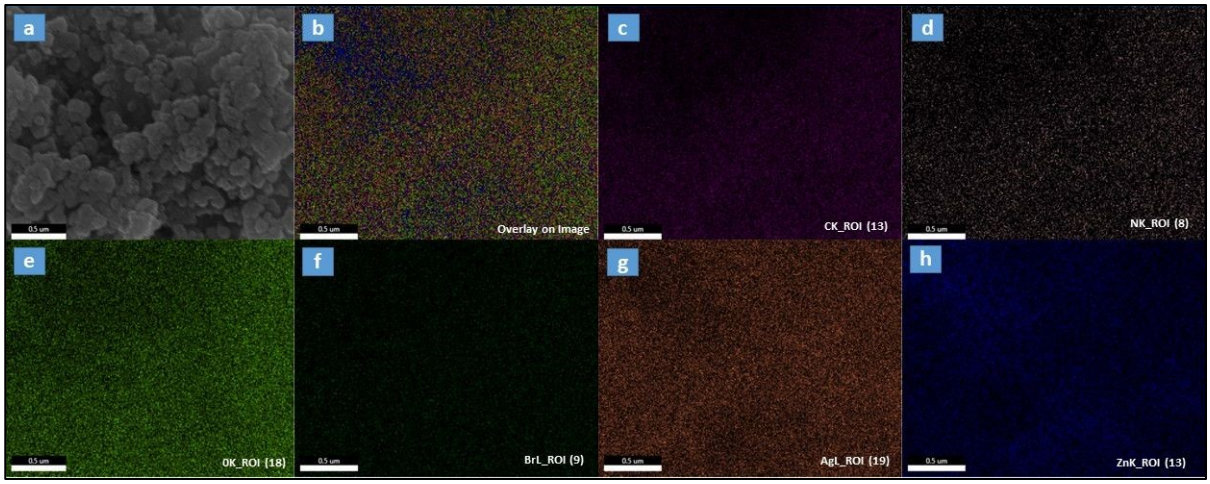

Figure 7. Elemental Mapping of ZnO@PDA@Ag@9-Br-Nos nanocomposite

5.1.5. *In vitro* 9-Br-Nos drug loading and release efficiency using HPLC

HPLC is a standard analytical method for determining the amount of drug loaded or the encapsulation efficiency in nanoparticle formulations. In this study, HPLC was utilized to assess the drug loading of 9-Br-Nos within ZnO@PDA@Ag@9-Br-Nos nanocomposites. The retention time identified for 9-Br-Nos was 3.5 minutes. The calibration curve for this drug **(Figure 8a)** was linear over concentrations ranging from 100 to 400 µg/mL, with a regression equation of Y = 0.0495X – 1.35632 and a correlation coefficient (R^2) of 0.9932. By applying this equation to the chromatogram peak areas from the nanocomposite sample **(Figure 8c)**, the drug loading was calculated to be 69.40% for 9-Br-Nos in the ZnO@PDA@Ag@9-Br-Nos system.[54] The drug loading on ZnO@PDA@Ag nanocomposite's is primarily controlled by non-covalent interactions. The 9-Br-Nos aromatic rings allow π–π stacking with the PDA coating's catechol and indole groups. Furthermore, hydrophobic interactions and hydrogen bonding between functional groups (–OH, –NH) support the drug's stable adsorption onto the nanocomposite surface.

The drug release study of ZnO@PDA@Ag@9-Br-Nos nanocomposites was performed in phosphate-buffered saline (1x PBS) at pH 7.4 and 5.5 to mimic physiological and tumor conditions. The 9-Br-Nos release profile from ZnO@PDA@Ag@9-Br-Nos nanocomposites showed pH-dependent behavior. At acidic pH (pH 5.5), the nanocomposite releases more drug than it does at physiological pH (pH 7.4). The release pattern exhibited a biphasic profile where there was an initial rapid burst drug release within the first 2-6 h,

View Article Online
DOI: 10.1039/D6NA00034G

likely due to desorption of drug molecules loosely bound on the surface. This was followed by a slower, sustained release phase, during which the drug release gradually increased to ~44% (pH 7.4) and ~47% (pH 5.5) over 48 h. The gradual disintegration of the nanocomposite structure and diffusion controlled drug transport via the PDA covering are reflected in this slower phase. Such a release profile is crucial for anticancer treatment because the sustained release helps to maintain effective drug concentrations over time, while the first burst rapidly reaches therapeutic drug levels at the tumor site. The hydrophobic '9-Br-Nos' bioavailability is increased by this regulated delivery, which also lowers systemic side effects and frequency of dosing, potentially enhancing therapeutic outcomes overall. The basic kinetic analysis of 9-Br-Nos drug-release behavior, including fitting to standard release models (zero-order, first-order, Higuchi, and Korsmeyer-Peppas), is provided in the Supporting Information (Figure S5) for detailed quantitative evaluation. With the highest correlation coefficients, the Korsmeyer-Peppas model demonstrated the best fit among them. The diffusion exponent ($n < 0.45$) indicates that Fickian diffusion is the primary mechanism governing the release of 9-Br-Nos from the nanocomposite. This suggests that drug release occurs mainly through diffusion from the PDA matrix, with enhanced release under acidic conditions (pH 5.5) due to partial destabilization of the nanocomposite.

View Article Online
DOI: 10.1039/D6NA00034G

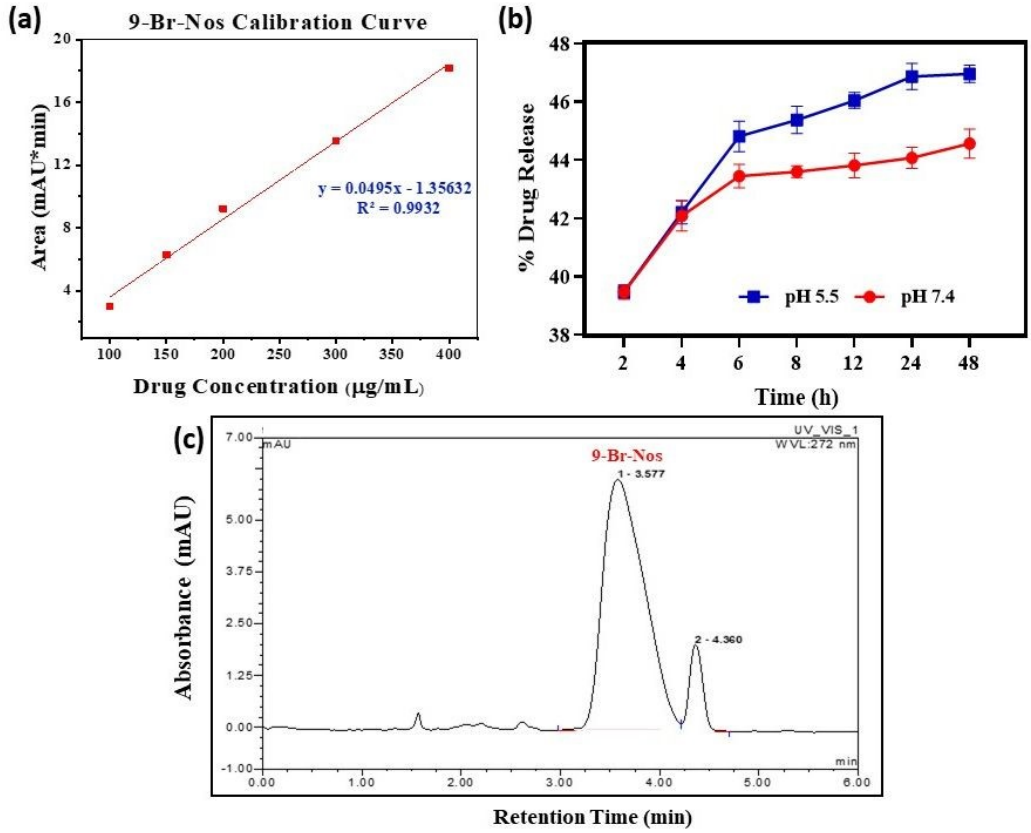

Figure 8. Represents (a) Calibration curve, (b) Drug Release Profile at pH 7.4 and 5.5, and (c) HPLC chromatogram depicting retention time of 9-Br-Nos drug

6.1. Cytotoxicity analysis by MTT Assay

To validate the use of ZnO@PDA@Ag@9-Br-Nos nanocomposite for biomedical applications, toxicity assessment was performed against human lung cancer cell line H1299 compared with normal HEK-293 kidney cells using the MTT assay **(Figure 9).** Free '9-Br-Nos', a hydrophobic drug with poor aqueous solubility, reduced H1299 cell viability to ~55% at 10 µg/mL concentration after 48 h treatment, confirming its inherent anticancer activity. However, the ZnO@PDA@Ag@9-Br-Nos nanocomposite, which is water dispersible due to the PDA polymer coating, exhibited a much stronger and dose-dependent cytotoxic effect, decreasing H1299 viability from ~70% at 10 µg/mL to ~25% at 100 µg/mL.

The IC_{50} of ZnO@PDA@Ag@9-Br-Nos nanocomposite on H1299 cells was calculated as 33.51 ± 4.54 µg/mL, which is lower than the IC_{50} value obtained for ZnO@PDA@Ag nanocomposite in our previous work (42.42 ± 4 µg/mL)[48], indicating enhanced cytotoxic

View Article Online
DOI: 10.1039/D6NA00034G

efficacy upon drug loading. In contrast, HEK-293 cells retained >75% viability even at the highest concentration, confirming good biocompatibility and selective cytotoxicity towards lung cancer cells. Statistical analysis showed highly significant differences (****$p < 0.0001$) in cell viability across treated groups of both H1299 and HEK-293 cells. Differences between treated groups and the control were indicated as ($^{\#}p < 0.05$, $^{\#\#}p < 0.01$, $^{\#\#\#}p < 0.001$, and $^{\#\#\#\#}p < 0.0001$. These findings highlight the potential of ZnO@PDA@Ag@9-Br-Nos as a water dispersible, selective nanotherapeutic system for lung cancer treatment.

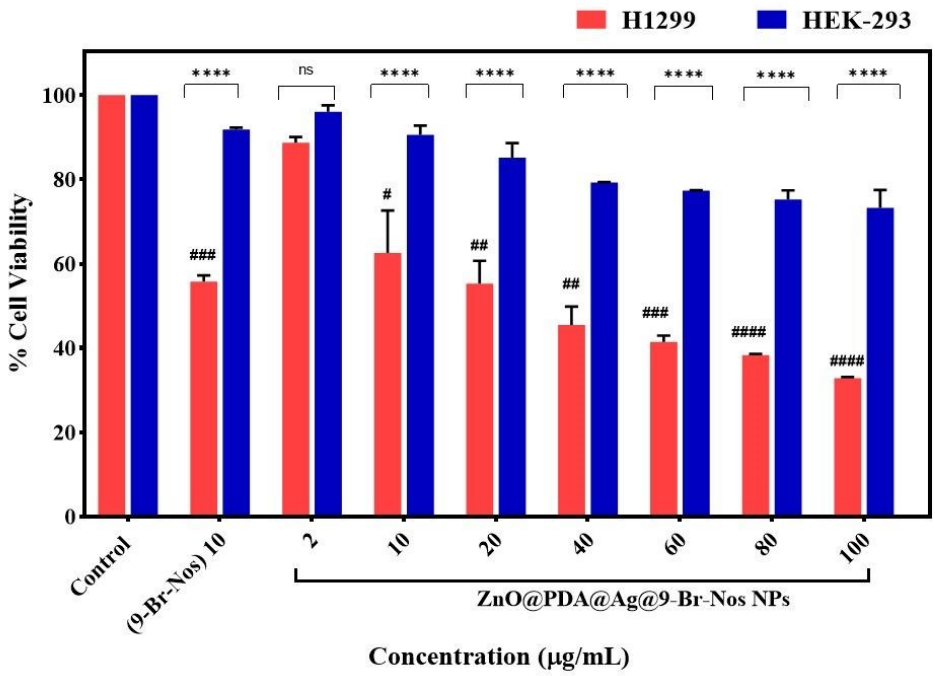

Figure 9. Graph showing comparative cytotoxic effect of ZnO@PDA@Ag@9-Br-Nos nanocomposite against H1299 and HEK-293 Cells.

6.2. Nanoparticle-Induced Morphology Changes in H1299 Cells

Phase-contrast microscopy (20×) revealed distinct morphological differences between control and treated H1299 cells after 48 h. Untreated or control cells retained the normal epithelial-like, polygonal morphology, and intact cell-cell contacts (**Figure 10a)**. However, the cells treated with 9-Br-Nos at its IC_{50} concentration (10 µg/mL) showed reduced confluence, rounding, and partial detachment, along with visible extracellular precipitates of the drug, consistent with its poor aqueous solubility (**Figure 10b)**.[55]

View Article Online
DOI: 10.1039/D6NA00034G

These observations indicate cytotoxic effects of the free drug but also suggest limitations in its bioavailability. In contrast, H1299 cells treated with ZnO@PDA@Ag@9-Br-Nos nanocomposites as shown in (**Figure 10c)** at their ~IC_{50} concentration (30 µg/mL) displayed pronounced morphological alterations. These includes extensive rounding, cell shrinkage, loss of adhesion, and floating cells, indicating mid to late-stage apoptotic changes. Unlike the free drug, no precipitation can be seen in case of nanocomposite treated, confirming enhanced cytotoxicity, improved solubility and drug delivery offered by the nanocomposite as compared to the free drug.

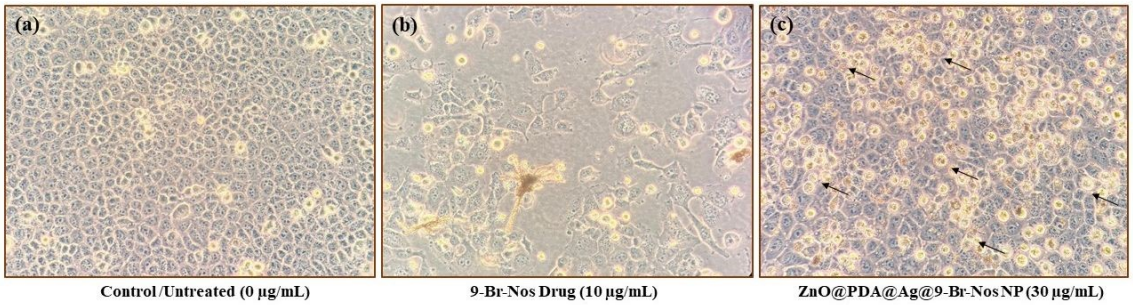

Figure 10. Phase-contrast microscopy (20×) images showing morphological alteration in H1299 cells after 48 h of treatment with (b) free drug and (c) ZnO@PDA@Ag@9-Br-Nos nanocomposites

6.3. Clonogenic Survival Assay

To further validate the cytotoxic potential and long-term proliferative capacity of of free 9-Br-Nos drug and its nanocomposite-based formulation ZnO@PDA@Ag@9-Br-Nos against H1299 cells, clonogenic assay was performed. As shown in **Figure 11a**, untreated control cells exhibited dense colony formation, confirming their high survival potential. Treatment with free 9-Br-Nos drug significantly reduced clonogenic survival to ~59.4% of the control at 2 µg/mL concentration, indicating strong inhibition of reproductive viability (**Figure 11b)**. In contrast, cells exposed to ZnO@PDA@Ag@9-Br-Nos nanocomposites demonstrated a concentration dependent reduction in colony formation at sub-IC_{50} levels, with survival fractions of ~85.4%, 72.6%, and 41.5% at 5 µg/mL (~0.15 × IC_{50}), 15 µg/mL (~0.45 × IC_{50}), and 25 µg/mL (~0.75 × IC_{50}) respectively. While the inhibition at the lowest concentration (5 µg/mL) was less pronounced compared to the free drug, the higher concentration (25 µg/mL) produced a

View Article Online
DOI: 10.1039/D6NA00034G

substantial suppression of colony formation as shown in **Figure 11 (c-e)**. This can be attributed to the sustained and controlled intracellular release of 9-Br-Nos drug from the ZnO@PDA@Ag nanocomposite, which prolongs cytotoxic effects and enhances long-term efficacy.

Overall, these findings confirm that ZnO@PDA@Ag@9-Br-Nos nanocomposite effectively suppress the clonogenic survival of H1299 cells in a dose-dependent manner. The stronger inhibition observed at higher concentrations highlights the therapeutic advantage of nanoparticle-mediated drug delivery compared to the free 9-Br-Nos drug.

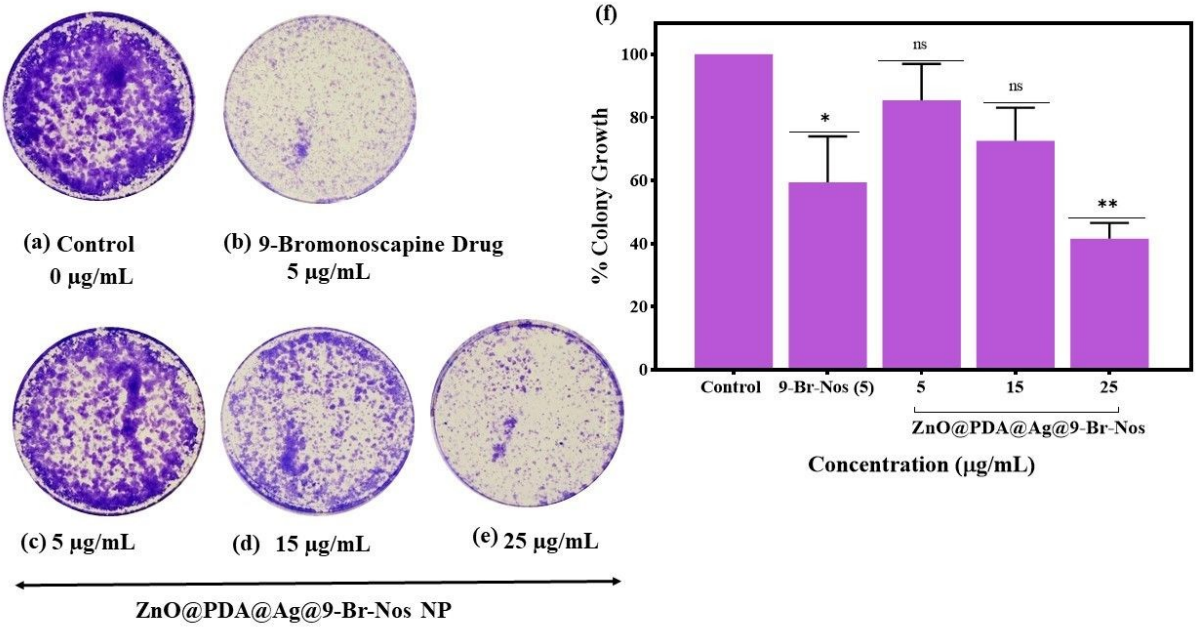

Figure 11. Clonogenic assay of H1299 cells showing colony formation in (a) control, (b) free drug, and (c-e) ZnO@PDA@Ag@9-Br-Nos nanocomposite treated; (f) Quantitative % colony growth relative to control.

6.4. Migration Inhibition Potential Assay

The anti-migratory potential of ZnO@PDA@Ag@9-Br-Nos nanocomposite was evaluated using a wound healing assay **(Figure 12)**. In the untreated control group, H1299 cells exhibited rapid wound gap closure, with nearly > 95% migration into the wound gap within 48 h **(Figure 12a)**. In contrast, cells treated with the positive control

View Article Online
DOI: 10.1039/D6NA00034G

'9-Br-Nos' drug (5 µg/mL) displayed reduction in cell migration after 24 and 48 h, consistent with its established microtubule-modulating properties.

Additionally, treatment with nanocomposite resulted in a dose and time dependent H1299 cells migration inhibition. At 5 µg/mL, a partial reduction in wound closure was observed, while at 15 and 25 µg/mL, a pronounced inhibition was evident, with wider wound gaps persisting even after 48 h. Quantitative analysis revealed a significant reduction in the percentage of wound closure compared to the untreated group, with 25 µg/mL treatment showing the strongest inhibitory effect **(Figure 12b).** These findings indicate that the prepared ZnO@PDA@Ag@9-Br-Nos nanocomposite effectively suppressed the migration of H1299 cells. The results highlight its potential to limit cancer metastasis and invasion, and suggesting its promise as a rapid therapeutic approach for lung cancer.

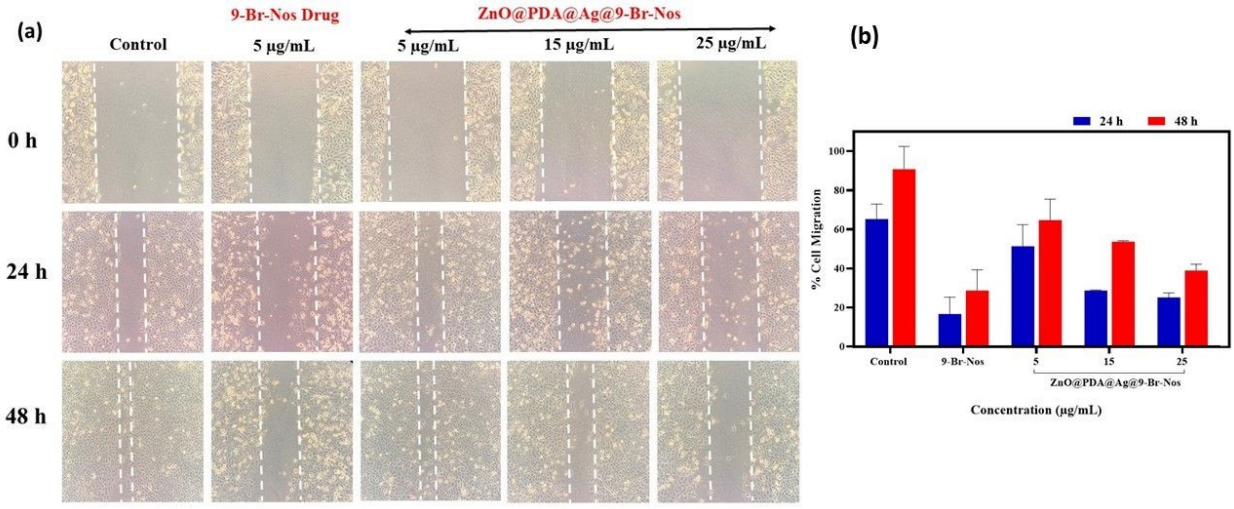

Figure 12. (a) Microscopic images (10x) of cell migration at 0, 24, and 48 h after treatment with free 9-Br-Nos and ZnO@PDA@Ag@9-Br-Nos compared to control on H1299 cells. (b) Quantitative analysis of % cell migration at 24 and 48 h.

6.5. Flow Cytometry Apoptosis Analysis

The apoptotic effects of free '9-Br-Nos' and its loaded nanocomposite form 'ZnO@PDA@Ag@9-Br-Nos' was assessed using flow cytometry based apoptosis study on H1299 cells. After 48 h treatment, the untreated or control group exhibited

View Article Online
DOI: 10.1039/D6NA00034G

predominantly 95.9% viable cells, with minimal early apoptosis (0.7%), late apoptosis (3.3%), and necrotic population (0.1%), confirming normal cell health in basal conditions **(Figure 13a)**. Treatment with 9-Br-Nos alone significantly increased the apoptotic fraction, to 33.8% while viable cells decreased to 66% as shown in **(Figure 13b)**. Furthermore, the ZnO@PDA@Ag@9-Br-Nos nanocomposite significantly increased apoptotic induction, with early apoptosis of 5% and late apoptosis reaching 67.5%, accompanied by a considerable decrease in the viability of cells to 22.3% **(Figure 13c)**. This synergistic apoptotic effect, further supported by quantitative bar-graph analysis, confirms that nano-enabled delivery of 9-Br-Nos substantially potentiates its anticancer efficacy. This synergistic apoptotic result is validated by quantitative bar-graph analysis **(Figure 13d)**, demonstrates that 9-Br-Nos is significantly more effective against lung cancer when delivered by nanocomposite. Overall, these results highlight the superior apoptotic activity of the ZnO@PDA@Ag mediated '9-Br-Nos' delivery system in comparison to the free drug, establishing the nanocomposite as a promising platform for enhanced and effective lung cancer therapy.

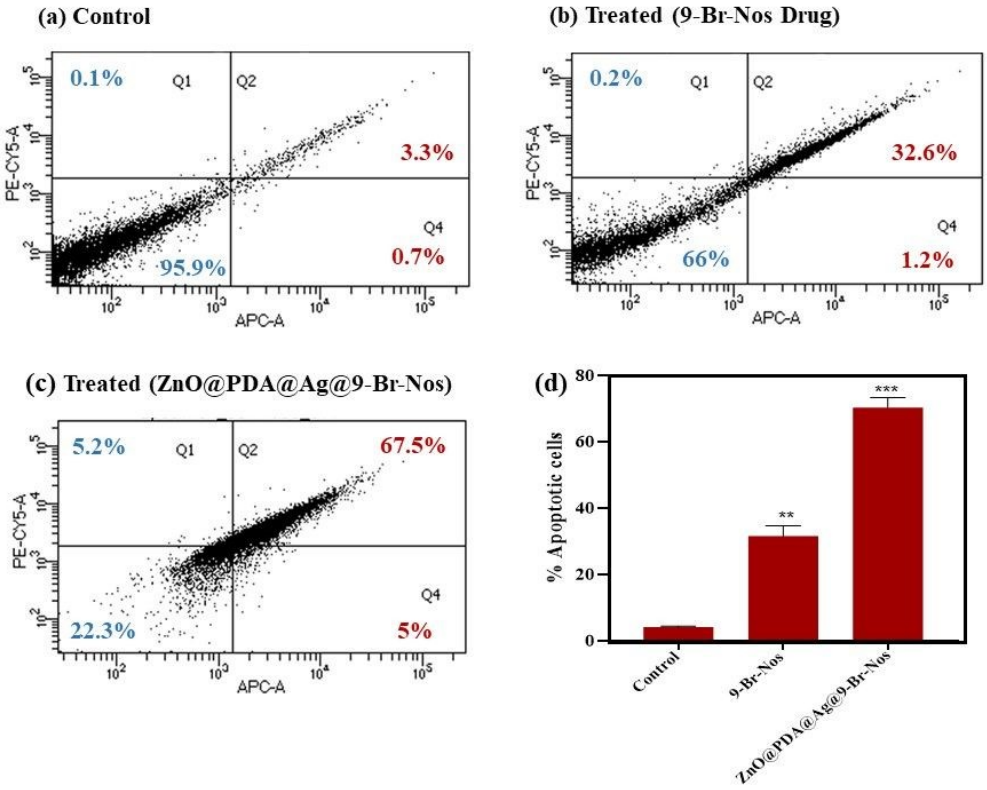

View Article Online
DOI: 10.1039/D6NA00034G

Figure 13: Cell Apoptosis Assay on H1299 cancer cells (a) Control, (b) free drug treated, (c) ZnO@PDA@Ag@9-Br-Nos treated, and (d) Bar graph depicting % Apoptotic cells.

6.6. *In vitro* Hemocompatibility Assessment by Hemolysis Assay

The hemocompatibility of ZnO@PDA@Ag@9-Br-Nos nanocomposite was assessed by a hemolysis assay using human red blood cells, with 1% Triton X-100 and 1x PBS serving as positive and negative controls, respectively. 1% Triton X-100 induced 100% hemolysis, while 1x PBS showed no hemolysis, confirming the stability of erythrocytes under physiological conditions. **Figure 14,** shows the nanocomposites exhibited a concentration-dependent hemolytic effect. The image shows visual confirmation of hemolysis in corresponding samples after centrifugation, where red coloration in the supernatant correlates with RBC lysis. At lower concentrations of 30 and 150 µg/mL, hemolysis was negligible (< 2-5%). However, with increasing concentrations, hemolysis gradually increased, reaching ~8% at 250 µg/mL to ~34% at 650 µg/mL. These results were further supported by the photographic evidence of RBC suspensions, which showed growing redness or lysis at higher dosages and clear supernatants at lower concentrations. Notably, at the IC_{50} value of 33.51 ± 4.54 µg/mL against H1299 lung cancer cells, the nanocomposite induced less than 2-5% hemolysis, demonstrating good selectivity towards cancer cells while maintaining blood compatibility. The findings indicate that the nanocomposite holds considerable potential for biomedical and therapeutic applications.

View Article Online
DOI: 10.1039/D6NA00034G

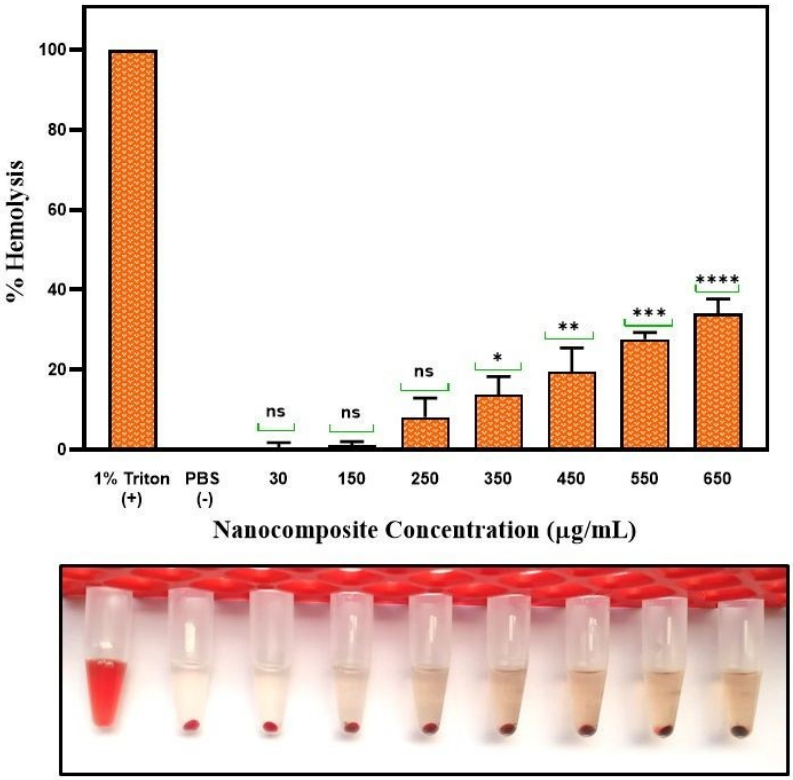

Figure 14. Biocompatibility assay of ZnO@PDA@Ag@9-Br-Nos nanocomposites assessed *via* hemolysis in human RBCs at various concentrations (30-650 µg/mL).

7. Limitations of the Study

In the present study, only hemolysis was performed for blood compatibility, while other parameters such as involving long-term cytotoxicity, platelet aggregation, oxidative stress, and inflammatory response were not evaluated. These assessments will be included in future investigations to achieve a more comprehensive evaluation of systemic biocompatibility. Additionally, *in vivo* toxicity and biodistribution analyses could not be performed due to the unavailability of ethical approval during the study period. This limitation restricted the evaluation of pharmacokinetics, organ accumulation, and long-term biocompatibility of the nanocomposite, which remain important directions for future investigation. Furthermore, the current synthesis method yields relatively small batch quantities, and scaling up the process may introduce

View Article Online
DOI: 10.1039/D6NA00034G

difference in particle size, polymer coating uniformity, and drug-loading efficiency, indicating the need for further optimization to enable larger-scale production.

8. Conclusion

This research work extends our previously developed ZnO@PDA@Ag nanocomposite synthesized *via* co-precipitation. To address limitations of conventional cancer therapies, a multifunctional ZnO@PDA@Ag system was employed as a nanocarrier for the hydrophobic drug 9-Br-Nos. The biological performance of the ZnO@PDA@Ag@9-Br-Nos nanocomposite is closely linked to its physicochemical properties. Its nanoscale size supports cellular uptake, while the negative zeta potential (−31.5 mV) ensures good stability and uniform dispersion in biological media, which is critical for effective interaction with cells. The presence of the PDA coating provides functional groups for efficient drug loading through non-covalent interactions, while also contributing to sustained drug release. Additionally, Ag nanoparticle decoration may further enhance therapeutic efficacy through synergistic effects. This combination subsequently increases cytotoxicity against lung cancer cells while also ensuring efficient medication release at the target site. ZnO@PDA@Ag@9-Br-Nos efficiently reduced H1299 lung cancer cell viability, colony formation, and migration, as demonstrated by *in vitro* MTT, clonogenic, and wound healing assays. This suggests that ZnO@PDA@Ag@9-Br-Nos has a great potential to limit tumor development and metastasis. Furthermore, the ZnO@PDA@Ag based 9-Br-Nos delivery system outperforms the free drug in terms of apoptotic activity. Importantly, cytotoxicity tests against HEK-293 normal cells and hemocompatibility against RBCs validated the nanocomposite's biocompatibility and safety, highlighting its potential for clinical use. Overall, our study establishes ZnO@PDA@Ag@9-Br-Nos as a promising platform for targeted lung cancer therapy. Through the integration of regulated drug administration, improved anticancer efficacy, and reduced off-target toxicity, this approach tackles important issues with traditional chemotherapy. Future research will focus on advancing this nanocomposite to *in vivo* evaluation by performing comprehensive pharmacokinetic, biodistribution, and acute and long-term toxic assessments in appropriate animal models. This could present a multipurpose, safe, and efficient

View Article Online
DOI: 10.1039/D6NA00034G

strategy to enhance lung cancer patient outcomes. Its multifunctional design highlights this nanocomposite's promise as a next-generation cancer treatment approach.

9. Ethical Approval and Informed Consent Statement

The hemolysis assays were performed in accordance with institutional ethical guidelines. Ethical clearance for the study was granted by the Institutional Ethical Committee (IEC) and Animal Ethics Committee of the Department of Chemistry, University of Delhi (IEC Approval Reference: 2237/CHEM, Date: 30-07-2020). The blood donor provided informed consent and approved the collection, preservation, and use of the samples for scientific research purposes.

10. Conflict of Interests

The authors have no conflict of interest to declare.

11. Acknowledgement

The authors acknowledge Dr. B. R. Ambedkar Center for Biomedical Research (ACBR), Institute of Nanomedical Sciences (INMS), and Department of Chemistry, University of Delhi to carry out the research work. We would like to acknowledge University Science Instrumentation Centre (USIC), University of Delhi and Vallabhbhai Patel Chest Institute, University of Delhi, India for providing the instrumentation facilities. T.G. is grateful for the award of DST-INSPIRE (IF200339) for financial assistance.

12. References

(1) 8703.00.Pdf. https://www.cancer.org/content/dam/CRC/PDF/Public/8703.00.pdf (accessed 2025-09-19).

(2) Sathishkumar, K.; Chaturvedi, M.; Das, P.; Stephen, S.; Mathur, P. Cancer Incidence Estimates for 2022 & Projection for 2025: Result from National Cancer Registry Programme, India. *Indian J. Med. Res.* **2022**, *156* (4 & 5), 598–607. https://doi.org/10.4103/ijmr.ijmr_1821_22.

View Article Online
DOI: 10.1039/D6NA00034G

(3) Chaitanya Thandra, K.; Barsouk, A.; Saginala, K.; Sukumar Aluru, J.; Barsouk, A. Epidemiology of Lung Cancer. *Contemp. Oncol. Onkol.* **2021**, *25* (1), 45–52. https://doi.org/10.5114/wo.2021.103829.

(4) Siegel, R. L.; Kratzer, T. B.; Giaquinto, A. N.; Sung, H.; Jemal, A. Cancer Statistics, 2025. *Ca* **2025**, *75* (1), 10–45. https://doi.org/10.3322/caac.21871.

(5) Kaur, R.; Bhardwaj, A.; Gupta, S. Cancer Treatment Therapies: Traditional to Modern Approaches to Combat Cancers. *Mol. Biol. Rep.* **2023**, *50* (11), 9663–9676. https://doi.org/10.1007/s11033-023-08809-3.

(6) Alavinejad, M.; Shirzad, M.; Javid-Naderi, M. J.; Rahdar, A.; Fathi-karkan, S.; Pandey, S. Smart Nanomedicines Powered by Artificial Intelligence: A Breakthrough in Lung Cancer Diagnosis and Treatment. *Med. Oncol.* **2025**, *42* (5), 134. https://doi.org/10.1007/s12032-025-02680-x.

(7) Sharma, A.; Shambhwani, D.; Pandey, S.; Singh, J.; Lalhlenmawia, H.; Kumarasamy, M.; Singh, S. K.; Chellappan, D. K.; Gupta, G.; Prasher, P.; Dua, K.; Kumar, D. Advances in Lung Cancer Treatment Using Nanomedicines. *ACS Omega* **2023**, *8* (1), 10–41. https://doi.org/10.1021/acsomega.2c04078.

(8) Pérez-Herrero, E.; Fernández-Medarde, A. Advanced Targeted Therapies in Cancer: Drug Nanocarriers, the Future of Chemotherapy. *Eur. J. Pharm. Biopharm.* **2015**, *93*, 52–79. https://doi.org/10.1016/j.ejpb.2015.03.018.

(9) Synergizing Nanotechnology with Biomedical and Biotechnology for Healthcare. In *Nanotechnology Applications for Industry 4.0*; CRC Press: Boca Raton, 2025; pp 108–145. https://doi.org/10.1201/9781003634553-5.

(10) Pourmadabi, M.; Omrani, Z.; Doustgani, A.; Yazdian, F.; Nourhashemi, M.; Ahmadi, T.; Rahdar, A.; Fathi-karkan, S.; Valizadeh, N.; Romanholo Ferreira, L. F. Machine Learning Models Predict pH-Responsive Drug Release from Liver-Targeted Agarose-CMC-CeO2 Nanocomposites: Liver-Targeted Antioxidant Strike. *J. Drug Deliv. Sci. Technol.* **2025**, *114*, 107555. https://doi.org/10.1016/j.jddst.2025.107555.

(11) Hasannia, M.; Abounoori, M.; Mahmoudian, F.; Rahdar, A.; Fathi-karkan, S.; Shirzad, M.; Pandey, S. Multifunctional Pluronic Nanomedicine: Bridging the Gap between Chemoresistance and Effective Cancer Therapy. *J. Drug Deliv. Sci. Technol.* **2026**, *120*, 108220. https://doi.org/10.1016/j.jddst.2026.108220.

View Article Online
DOI: 10.1039/D6NA00034G

(12) Kawish, S. M.; Sharma, S.; Gupta, P.; Ahmad, F. J.; Iqbal, M.; Alshabrmi, F. M.; Anwer, Md. K.; Fathi-karkan, S.; Rahdar, A.; Aboudzadeh, M. A. Nanoparticle-Based Drug Delivery Platform for Simultaneous Administration of Phytochemicals and Chemotherapeutics: Emerging Trends in Cancer Management. *Part. Part. Syst. Charact.* **2024**, *41* (12), 2400049. https://doi.org/10.1002/ppsc.202400049.

(13) Pourmadadi, M.; Abdouss, H.; Memarzadeh, A.; Abdouss, M.; Fathi-karkan, S.; Rahdar, A.; Díez-Pascual, A. M. Innovative Chitosan-Polyacrylic Acid-MoS2 Nanocomposite for Enhanced and pH-Responsive Quercetin Delivery. *Mater. Today Commun.* **2024**, *39*, 108724. https://doi.org/10.1016/j.mtcomm.2024.108724.

(14) Khoz, R.; Pourmadadi, M.; Yazdian, F.; Rahdar, A.; Razzaq, S.; Fathi-karkan, S.; Aboudzadeh, M. A. Quercetin-Loaded Gelatin/Agarose/Fe2O3 Hybrid Nanocarriers in a Microemulsion Matrix: Synthesis, Characterization, and Cancer Therapeutic Potential. *Mater. Today Commun.* **2025**, *46*, 112597. https://doi.org/10.1016/j.mtcomm.2025.112597.

(15) Gupta, A.; Patel, P.; Shah, S.; Patel, K. Nanocomposites in Focus: Tailoring Drug Delivery for Enhanced Therapeutic Outcomes. *Future J. Pharm. Sci.* **2025**, *11* (1), 37. https://doi.org/10.1186/s43094-025-00789-4.

(16) Tanino, R.; Amano, Y.; Tong, X.; Sun, R.; Tsubata, Y.; Harada, M.; Fujita, Y.; Isobe, T. Anticancer Activity of ZnO Nanoparticles against Human Small-Cell Lung Cancer in an Orthotopic Mouse Model. *Mol. Cancer Ther.* **2020**, *19* (2), 502–512. https://doi.org/10.1158/1535-7163.MCT-19-0018.

(17) Mousavi, M. S.; Pourmadadi, M.; Abdouss, M.; Rahdar, A.; Fathi-Karkan, S.; Pandey, S. Gelatin/ CMC /HAP Nanocomposites Based on Double Micro-Emulsion for Delivery of 5-FU: Synthesis and Chemical–Physical Characterization. *BioNanoScience* **2024**, *14* (5), 5513–5526. https://doi.org/10.1007/s12668-024-01515-9.

(18) Lebaka, V. R.; Ravi, P.; Reddy, M. C.; Thummala, C.; Mandal, T. K. Zinc Oxide Nanoparticles in Modern Science and Technology: Multifunctional Roles in Healthcare, Environmental Remediation, and Industry. *Nanomaterials* **2025**, *15* (10), 754. https://doi.org/10.3390/nano15100754.

(19) Anjum, S.; Hashim, M.; Malik, S. A.; Khan, M.; Lorenzo, J. M.; Abbasi, B. H.; Hano, C. Recent Advances in Zinc Oxide Nanoparticles (ZnO NPs) for Cancer Diagnosis, Target

View Article Online
DOI: 10.1039/D6NA00034G

Drug Delivery, and Treatment. *Cancers* **2021**, *13* (18), 4570. https://doi.org/10.3390/cancers13184570.

(20) Tseriotis, V.-S.; Ampazis, D.; Karachrysafi, S.; Papamitsou, T.; Petrakis, G.; Kouvelas, D.; Mavropoulos, P.; Lallas, K.; Sič, A.; Fouskas, V.; Stergiou, K.; Pavlidis, P.; Arnaoutoglou, M. ZnO-Based Nanoparticles for Targeted Cancer Chemotherapy and the Role of Tumor Microenvironment: A Systematic Review. *Int. J. Mol. Sci.* **2025**, *26* (17), 8417. https://doi.org/10.3390/ijms26178417.

(21) Lakshmipriya, T.; Gopinath, S. C. B.; Rajasingam, M.; Arun, S. I.; Fakhri, M. A.; Salim, E. T. Advancements With Zinc Oxide Nanomaterials: From Green Chemistry to Biomedical Applications. *BioNanoScience* **2026**, *16* (5), 310. https://doi.org/10.1007/s12668-026-02549-x.

(22) Akhtar, M. J.; Ahamed, M.; Kumar, S.; Khan, M. M.; Ahmad, J.; Alrokayan, S. A. Zinc Oxide Nanoparticles Selectively Induce Apoptosis in Human Cancer Cells through Reactive Oxygen Species. *Int. J. Nanomedicine* **2012**, *7*, 845–857. https://doi.org/10.2147/IJN.S29129.

(23) Keerthana, S.; Kumar, A. Potential Risks and Benefits of Zinc Oxide Nanoparticles: A Systematic Review. *Crit. Rev. Toxicol.* **2020**, *50* (1), 47–71. https://doi.org/10.1080/10408444.2020.1726282.

(24) Ragu Prasath, A.; Selvam, K. A Review of the Zinc Oxide Nanoparticles Synthesis and Their Emerging Biomedical Potential. *Biomed. Mater. Devices* **2025**. https://doi.org/10.1007/s44174-025-00422-1.

(25) Chandra Kanth, P.; Verma, S. K.; Gour, N. Functionalized Nanomaterials for Biomedical and Agriculture Industries. In *Handbook of Functionalized Nanomaterials for Industrial Applications*; Elsevier, 2020; pp 231–265. https://doi.org/10.1016/B978-0-12-816787-8.00010-7.

(26) Das, A.; Ghosh, S.; Bisal, P.; Pramanik, N. Doxorubicin (DOX) Modified Zinc Oxide (ZnO) Nanocomposite Encapsulated with Polymethyl Methacrylate (PMMA) Biopolymer for Effective Cancer Treatment. *Results Surf. Interfaces* **2025**, *18*, 100389. https://doi.org/10.1016/j.rsurfi.2024.100389.

(27) Amirsoleimani, A.; Bahrami, Z.; Kafshdouzan, K. Rice Bran Extract-Assisted Synthesis of PMO/ZnO Nanocomposites for Enhanced Gemcitabine Loading and Anticancer

View Article Online
DOI: 10.1039/D6NA00034G

Efficacy. *J. Drug Deliv. Sci. Technol.* **2025**, *114*, 107515. https://doi.org/10.1016/j.jddst.2025.107515.

(28) Hu, C.; Du, W. Zinc Oxide Nanoparticles (ZnO NPs) Combined with Cisplatin and Gemcitabine Inhibits Tumor Activity of NSCLC Cells. *Aging* **2020**, *12* (24), 25767–25777. https://doi.org/10.18632/aging.104187.

(29) Kazemi, A.; Afshari, M. H.; Baesmat, H.; Keshavarz, S.; Zeinali, F.; Zahiri, S.; Torabi, E.; Manteghi, F.; Rohani, S. Room-Temperature Synthesis of pH-Responsive MOF Nanocarriers for Targeted Drug Delivery in Cancer Therapy. *J. Polym. Environ.* **2025**, *33* (3), 1505–1516. https://doi.org/10.1007/s10924-025-03496-6.

(30) Kazemi, A.; Afshari, M. H.; Baesmat, H.; Bozorgnia, B.; Manteghi, F.; Nabipour, H.; Rohani, S.; Aliabadi, H. A. M.; Adibzadeh, S.; Saeb, M. R. Polydopamine-Coated Zn-MOF-74 Nanocarriers: Versatile Drug Delivery Systems with Enhanced Biocompatibility and Cancer Therapeutic Efficacy. *J. Inorg. Organomet. Polym. Mater.* **2024**, *34* (12), 5718–5731. https://doi.org/10.1007/s10904-024-03173-6.

(31) Noor, S.; Choudhury, A.; Islam, K. U.; Yousuf, Mohd.; Raza, A.; Ansari, M. A.; Ashraf, A.; Hussain, A.; Hassan, M. I. Investigating the Chemo-Preventive Role of Noscapine in Lung Carcinoma via Therapeutic Targeting of Human Aurora Kinase B. *Mol. Cell. Biochem.* **2025**, *480* (2), 1137–1153. https://doi.org/10.1007/s11010-024-05036-7.

(32) Chougule, M. B.; Patel, A. R.; Jackson, T.; Singh, M. Antitumor Activity of Noscapine in Combination with Doxorubicin in Triple Negative Breast Cancer. *PLoS ONE* **2011**, *6* (3), e17733. https://doi.org/10.1371/journal.pone.0017733.

(33) Yang, Y.; Ran, J.; Sun, L.; Sun, X.; Luo, Y.; Yan, B.; Tala; Liu, M.; Li, D.; Zhang, L.; Bao, G.; Zhou, J. CYLD Regulates Noscapine Activity in Acute Lymphoblastic Leukemia via a Microtubule-Dependent Mechanism. *Theranostics* **2015**, *5* (7), 656–666. https://doi.org/10.7150/thno.10844.

(34) Jhaveri, N.; Cho, H.; Torres, S.; Wang, W.; Schönthal, A. H.; Petasis, N. A.; Louie, S. G.; Hofman, F. M.; Chen, T. C. Noscapine Inhibits Tumor Growth in TMZ-Resistant Gliomas. *Cancer Lett.* **2011**, *312* (2), 245–252. https://doi.org/10.1016/j.canlet.2011.08.015.

(35) Chandra, R. Noscapine as Anticancer Agent & Its Role in Ovarian Cancer. *Org. Med. Chem. Int. J.* **2019**, *9* (02). https://doi.org/10.19080/OMCIJ.2019.09.555757.

View Article Online
DOI: 10.1039/D6NA00034G

(36) Zhou, J.; Panda, D.; Landen, J. W.; Wilson, L.; Joshi, H. C. Minor Alteration of Microtubule Dynamics Causes Loss of Tension across Kinetochore Pairs and Activates the Spindle Checkpoint. *J. Biol. Chem.* **2002**, *277* (19), 17200–17208. https://doi.org/10.1074/jbc.M110369200.

(37) DeBono, A.; Capuano, B.; Scammells, P. J. Progress Toward the Development of Noscapine and Derivatives as Anticancer Agents. *J. Med. Chem.* **2015**, *58* (15), 5699–5727. https://doi.org/10.1021/jm501180v.

(38) Newcomb, E. W.; Lukyanov, Y.; Smirnova, I.; Schnee, T.; Zagzag, D. Noscapine Induces Apoptosis in Human Glioma Cells by an Apoptosis-Inducing Factor-Dependent Pathway. *Anticancer. Drugs* **2008**, *19* (6), 553–563. https://doi.org/10.1097/CAD.0b013e3282ffd68d.

(39) Jyoti, K.; Kaur, K.; Pandey, R. S.; Jain, U. K.; Chandra, R.; Madan, J. Inhalable Nanostructured Lipid Particles of 9-Bromo-Noscapine, a Tubulin-Binding Cytotoxic Agent: In Vitro and in Vivo Studies. *J. Colloid Interface Sci.* **2015**, *445*, 219–230. https://doi.org/10.1016/j.jcis.2014.12.092.

(40) Department of Biotechnology & Bioinformatics, Sambalpur University, Jyoti Vihar – 768 019, Sambalpur, Odisha; Meher, R. K.; Naik, M. R.; Department of Pharmacology, VSS Institute of Medical Science & Research, Burla, Sambalpur, Odisha; Bastia, B.; Environmental Toxicology & Electron Microscope Lab, ICMR-National Institute of Pathology, Safdarjung Hospital Campus, New Delhi-110029, India; Naik, P. K.; Department of Pharmacology, VSS Institute of Medical Science & Research, Burla, Sambalpur, Odisha. Comparative Evaluation of Anti-Angiogenic Effects of Noscapine Derivatives. *Bioinformation* **2018**, *14* (05), 236–240. https://doi.org/10.6026/97320630014236.

(41) Zhou, J.; Gupta, K.; Aggarwal, S.; Aneja, R.; Chandra, R.; Panda, D.; Joshi, H. C. Brominated Derivatives of Noscapine Are Potent Microtubule-Interfering Agents That Perturb Mitosis and Inhibit Cell Proliferation. *Mol. Pharmacol.* **2003**, *63* (4), 799–807. https://doi.org/10.1124/mol.63.4.799.

(42) Awasthi, A.; Singh, M.; Rathee, G.; Chandra, R. Recent Advancements in Synthetic Methodologies of 3-Substituted Phthalides and Their Application in the Total Synthesis of

View Article Online
DOI: 10.1039/D6NA00034G

Biologically Active Natural Products. *RSC Adv.* **2020**, *10* (21), 12626–12652. https://doi.org/10.1039/D0RA00701C.

(43) Sewariya, S.; Sehrawat, H.; Mishra, N.; Singh, M. B.; Singh, P.; Kukreti, S.; Chandra, R. Comparative Assessment of 9-Bromo Noscapine Ionic Liquid and Noscapine: Synthesis, in-Vitro Studies plus Computational & Biophysical Evaluation with Human Hemoglobin. *Int. J. Biol. Macromol.* **2023**, *247*, 125791. https://doi.org/10.1016/j.ijbiomac.2023.125791.

(44) Porcù, E.; Sipos, A.; Basso, G.; Hamel, E.; Bai, R.; Stempfer, V.; Udvardy, A.; Bényei, A. Cs.; Schmidhammer, H.; Antus, S.; Viola, G. Novel 9′-Substituted-Noscapines: Synthesis with Suzuki Cross-Coupling, Structure Elucidation and Biological Evaluation. *Eur. J. Med. Chem.* **2014**, *84*, 476–490. https://doi.org/10.1016/j.ejmech.2014.07.050.

(45) Bhoi, N.; Pradhan, L. K.; Sahoo, D. R.; Pradhan, M. K.; Mohanta, P. P.; Pragyandipta, P.; Baitharu, I.; Naik, P. K. Potent Therapeutic Efficacy of 9-Bromo-Noscapine Against Breast Cancer Cells Via Enhanced Bioavailability of the Noscapine-Cyclodextrin Inclusion Complex. *Drug Dev. Res.* **2026**, *87* (1), e70208. https://doi.org/10.1002/ddr.70208.

(46) Wu, R.; Wang, H.; Hai, L.; Wang, T.; Hou, M.; He, D.; He, X.; Wang, K. A Photosensitizer-Loaded Zinc Oxide-Polydopamine Core-Shell Nanotherapeutic Agent for Photodynamic and Photothermal Synergistic Therapy of Cancer Cells. *Chin. Chem. Lett.* **2020**, *31* (1), 189–192. https://doi.org/10.1016/j.cclet.2019.05.004.

(47) Fedorenko, V.; Damberga, D.; Grundsteins, K.; Ramanavicius, A.; Ramanavicius, S.; Coy, E.; Iatsunskyi, I.; Viter, R. Application of Polydopamine Functionalized Zinc Oxide for Glucose Biosensor Design. *Polymers* **2021**, *13* (17), 2918. https://doi.org/10.3390/polym13172918.

(48) Goel, T.; Deshwal, N.; Gusain, S.; Chandra, R.; Tiwari, M.; Singh, S. Synthesis, Characterisation of ZnO@PDA@Ag Nanocomposite: Mechanistic Interaction with BSA, Photodegradation Activity & in Vitro Cytotoxicity Assay on H1299 Lung Cancer Cell Line. *Int. J. Biol. Macromol.* **2024**, *283*, 137532. https://doi.org/10.1016/j.ijbiomac.2024.137532.

(49) Singh, S.; Goel, T.; Singh, A.; Chugh, H.; Chakraborty, N.; Roy, I.; Tiwari, M.; Chandra, R. Synthesis and Characterization of Fe_3O_4 @SiO_2 @PDA@Ag Core–Shell Nanoparticles and Biological Application on Human Lung Cancer Cell Line and Antibacterial Strains. *Artif. Cells Nanomedicine Biotechnol.* **2024**, *52* (1), 46–58. https://doi.org/10.1080/21691401.2023.2295534.

View Article Online
DOI: 10.1039/D6NA00034G

(50) Ali, Md. H.; Azad, Md. A. K.; Khan, K. A.; Rahman, Md. O.; Chakma, U.; Kumer, A. Analysis of Crystallographic Structures and Properties of Silver Nanoparticles Synthesized Using PKL Extract and Nanoscale Characterization Techniques. *ACS Omega* **2023**, *8* (31), 28133–28142. https://doi.org/10.1021/acsomega.3c01261.

(51) Roy, H.; Maddiboyina, B.; Nayak, B. S.; Bohara, R. A. Novel Delivery Strategy: Finasteride-Loaded Solid Lipid Nanoparticles for Improved Androgenetic Alopecia Therapy. *RSC Adv. 15* (23), 18715–18731. https://doi.org/10.1039/d5ra00399g.

(52) Mousavi-Kouhi, S. M.; Beyk-Khormizi, A.; Amiri, M. S.; Mashreghi, M.; Taghavizadeh Yazdi, M. E. Silver-Zinc Oxide Nanocomposite: From Synthesis to Antimicrobial and Anticancer Properties. *Ceram. Int.* **2021**, *47* (15), 21490–21497. https://doi.org/10.1016/j.ceramint.2021.04.160.

(53) Fedorenko, V.; Viter, R.; Mrówczyński, R.; Damberga, D.; Coy, E.; Iatsunskyi, I. Synthesis and Photoluminescence Properties of Hybrid 1D Core–Shell Structured Nanocomposites Based on ZnO/Polydopamine. *RSC Adv.* **2020**, *10* (50), 29751–29758. https://doi.org/10.1039/D0RA04829A.

(54) Singh, S.; Sewariya, S.; Goel, T.; Panchal, S.; Singh, A.; Kukreti, S.; Tiwari, M.; Chandra, R. Assessing Dual Drug 9-Hydroxymethyl Noscapine and Telmisartan-Loaded Stearic Acid Nanoparticles against (H1299) Non-Small Cell Lung Cancer and Their Mechanistic Interaction with Bovine Serum Albumin. *Mater. Adv.* **2025**, *6* (4), 1364–1378. https://doi.org/10.1039/D4MA00958D.

(55) Chugh, H.; Mishra, N.; Chandra, S.; Sharma, J. G.; Chandra, R. Noscapine-Loaded Collagen-Based Silver Nanoparticles: A Potent Nano-Therapeutic Approach for Cancer Treatment. *RSC Adv.* **2025**, *15* (40), 33264–33277. https://doi.org/10.1039/D5RA03766B.

View Article Online
DOI: 10.1039/D6NA00034G

ZnO@PDA@Ag Nanocomposite-Mediated Delivery of 9-Bromonoscapine, an Anticancer Agent, for Enhanced Lung Cancer Therapy

Data Availability Statement

The authors declare that the data supporting the findings of this study are provided within the article. Additional raw data are available from the corresponding author upon reasonable request.